The Salaverry forearc basin, offshore Peru: Neogene evolution based on seismic sequence stratigraphy

Oscar López-Gamundí[1]

[1]P1Consultants LLC, 1121 A Banks Stret, Houston, TX, 77006, USA
olopez-gamundi@p1consultants.com

Abstract

Using integrated 3D seismic data and regional 2D seismic lines, this study establishes the seismic stratigraphic framework of the Miocene-Pliocene succession in the central Salaverry forearc basin, offshore Peru. The basin fill is divided into three megasequences: (1) R, characterized by alternating amplitude reflectors under underfilled conditions; (2) S, a thin, largely seismically transparent unit containing basal channel-levee complexes formed under sediment-starved conditions; and (3) C-MTC, comprising deltaic clinoforms and mass-transport deposits that record overfilled conditions during Pliocene uplift of the oceanward Outer Shelf High (OSH). The megasequences are further subdivided into depositional sequences (A to F) whose stratal terminations record the interplay of tectonic subsidence, basin inversion, and two distinct phases of OSH uplift. Seismic stratigraphic analysis indicates that erosion of sequences A and B along the seaward margin of the Salaverry Basin records the onset of OSH uplift. Overlying sequences C-F exhibit progressive changes in stratal architecture, including truncation, onlap, draping, and thickening across the eastern flank of the OSH into the adjacent Trujillo Basin. Thickening of sequences E and F reflects increasing subsidence from late sequence E onward, with deposition occurring during relative tectonic quiescence. Amplitude mapping delineates major sand fairways, including transgressive basal sands, sinuous channels and terminal splays (sequence B), isolated shelf sands (sequence E), and channel-levee complexes (sequence F). Basin fill was initially underfilled, with sediment supplied from the east. Axial sediment transport developed during the final stages of basin evolution, indicating increased basin confinement and overfilled conditions associated with continued uplift of the OSH.

Keywords: Forearc basins, Offshore Peru, Seismic sequence stratigraphy, Stratal terminations, Outer arc high, Deepwater deposits

La cuenca de antearco de Salaverry, costa afuera de Perú: evolución neógena basada en estratigrafía secuencial sísmica. Este estudio establece, mediante la integración de datos sísmicos 3D integrados y líneas sísmicas 2D regionales, el marco sismoestratigráfico de la sucesión mio-pliocena en la cuenca de antearco de Salaverry, frente a la costa de Perú. El relleno de la cuenca se puede dividir en tres megasecuencias: (1) R, caracterizada por reflectores de amplitud alternante bajo condiciones de equilibrio entre espacio de acomodación y aporte sedimentario; (2) S, una unidad delgada y sísmicamente transparente que contiene complejos de canales en su base formados bajo condiciones mayoritariamente de subllenado; y (3) C-MTC, que incluye clinoformas deltaicas y depósitos de transporte en masa que registran condiciones de sobrellenado durante el levantamiento plioceno del alto externo (*Outer Shelf High*, *OSH*). Estas megasecuencias se subdividen en secuencias depositacionales (A-F) cuyas terminaciones estratales reflejan la interacción entre la subsidencia tectónica, la inversión de la cuenca y dos fases de levantamiento del OSH. El análisis sismoestratigráfico indica que la erosión de las secuencias A y B a lo largo del margen occidental de la cuenca registra el inicio del levantamiento del OSH. Las secuencias suprayacentes C-F muestran cambios progresivos en su arquitectura estratal, lo cual incluye truncamiento, superposición, recubrimiento y engrosamiento a lo largo del flanco oriental del OSH hacia la cuenca de Trujillo. El engrosamiento de las secuencias E y F refleja un aumento de la subsidencia desde finales de la secuencia E, con sedimentación durante periodos de relativa calma tectónica. El mapeo de amplitud delimita las principales vías de arena, incluyendo arenas basales transgresivas, canales sinuosos y abanicos terminales (secuencia B), arenas aisladas de plataforma (secuencia E) y complejos de canales (secuencia F). El relleno de la cuenca fue inicialmente insuficiente, con sedimentos suministrados desde el este. El transporte axial de sedimentos se desarrolló durante las etapas finales de la evolución de la cuenca, lo que indica un aumento en el confinamiento de esta y condiciones de sobrellenado asociadas con el levantamiento continuo del OSH.

Palabras clave: cuencas de antearco, costa afuera de Perú, estratigrafía secuencial sísmica, terminaciones estratales, alto externo, depósitos de aguas profundas

1. Introduction

Forearc basins develop within arc-trench gaps between the axes of trenches, which mark subduction zones, and the parallel magmatic arcs or structural backstops (Dickinson, 1973, 1974, 1995; Karig, 1974; Seely et al., 1974; Karig and Sharman, 1975; Ingersoll, 1988; Draut and Clift, 2012; Roeder, 2012). The stratigraphic and tectonic characteristics of these basins record the long-term interactions between subducting and overriding plates along convergent margins (Noda, 2016). Forearc basins typically form on the landward side of accretionary prisms, where basin margins progressively migrate seaward as the accretionary prism (outer wedge) grows. The seaward edge of a forearc basin overlaps an elevated slope ridge and plays a significant role in regulating sediment supply (Beaudry and Moore, 1985; Moxon and Graham, 1987; Dickinson, 1995; van der Werff, 1996; Fildani et al., 2008; Takano et al., 2013; Buchs et al., 2015; Noda and Miyakawa, 2017; Takano, 2017; Kimura et al., 2018; Menant, 2020). In forearc basins accommodation space is primarily of tectonic nature (tectonically induced subsidence or uplift), whereas morphological internal variations include underfilled and overfilled stages, with outer ridges that may be either emerged or submerged (Seely, 1979; Dickinson and Seely, 1979; Dickinson, 1995). Overfilled stages are common in forearc basins adjacent to continental margins.

In the Andes between 5° and 35° S, forearc basins characterized by the absence of an accretionary wedge in a subduction erosion context are common (Rutland, 1971; Kulm et al., 1977; Macharé et al., 1986; Kukowski and Oncken, 2006; Calvès et al., 2017). The Salaverry Basin in central Peru is one of such basins (Fig. 1). These forearc basins exhibit a complex structural history; for example, shelf basins like Salaverry are bounded by the continent to the east and an outer ridge to the west, whereas the neighboring but farther offshore Trujillo and Lima basins lie between two trench-parallel ridges, named in the literature as Outer Shelf High (OSH) and Upper Slope Ridge (USR) (Thornburg and Kulm, 1981; Kulm et al., 1981, 1982; Thornburg, 1985; von Heune et al., 1986) (Figs. 1 and 2).

Based on the unusual structural characteristics of the forearc basins of central Peru, this study presents a comprehensive regional seismic sequence stratigraphic evaluation of the central Salaverry Basin. By integrating regional seismic reflection data with sequence stratigraphic principles, the study seeks to establish a robust stratigraphic framework for the Miocene-Pliocene interval and characterize the spatial and temporal distribution of depositional sequences across the basin. The primary objective is to elucidate the tectonic evolution of the basin and identify the principal sediment pathways that controlled sediment delivery. Additionally, this study aims to evaluate the relationship between structural elements and sedimentary processes, thereby improving the understanding of basin evolution within the forearc setting of central Peru. The resulting seismic stratigraphic framework is intended to provide new insights into the interplay between tectonics and sedimentation, refine regional geological correlations, and contribute to a better understanding of the Neogene geological evolution of the Peruvian forearc margin.

2. Regional setting of the Salaverry Basin

The development of the forearc basins offshore Peru was controlled by the interaction between the Nazca-Farallon (oceanic) and South American (continental) plates, along with the subduction of the Nazca Ridge. The offshore region of Peru consists of a series of forearc basin trends formed along the continental shelf (Fig. 1). A submarine basement high: *i.e.*, the OSH (Kulm et al., 1982; Romero et al., 2013), also known as the Salaverry-

Trujillo High (Azalgara, 1993), Paracas Arch (Benavides, 1999), Paracas High (Ramos, 2009), and Salaverry High (PARSEP, 2001a; Genge et al., 2020), consisting of metamorphic and crystalline Paleozoic and Proterozoic rocks, separates both basin trends. This submerged structural high, considered by some authors as the offshore submarine continuation of the Coastal Cordillera (Prudhomme et al., 2019), is a prominent feature formed by significant Late Miocene uplift and further accentuated by additional uplift during the Pliocene (PARSEP, 2001a). In his regional study of the offshore basins of Peru, Azalgara (1993) proposed that the OSH "*began to form by the end of the middle Miocene and proceed until Pliocene"* and described it as a "*370 km long, trench parallel open flexure and, in part, a 60 km long, parallel belt of anticlines*". The Salaverry, Sechura, Talara, and East Pisco basins form part of the inner basin trend, located between the OSH and the South American continental plate, whereas the outer trend, situated west of the OSH, includes the Trujillo, Lima, and West Pisco basins (Thornburg and Kulm, 1981; Marty, 1989; Dunbar et al., 1990).

Paleozoic and Mesozoic rocks form the basement of the forearc basins (Romero et al., 2010). For example, samples taken from cuttings of the San Miguel 1X well in the offshore Sechura Basin (see location in figure 1) have gabbro-dioritic compositions and yield Permian (259.5±12.3 Ma; $^{40}Ar/^{39}Ar$) ages, whereas an Ordovician age (467.9±4.5 Ma; U-Pb) was obtained for an orthogneiss exposed on the Las Hormigas de Afuera Island, between the southernmost end of the Salaverry Basin and the East Pisco Basin (Romero et al., 2013). The age of the Cenozoic sediments was determined from micropaleontological analyses from the Delfin 1X and Ballena 1X wells (Valdespino and Seminario, 1976a, b; Schell, 1978; Okada, 1990; Schrader and Cruzado, 1990; PeruPetro 1981a, b; Canchanya and Paz, 1992; Narvaez and Pardo, 1993; Morales and Gonzales, 2006; Gonzales, 2014). In addition to age dating, Okada (1990) inferred paleobathymetric zonations for the stratigraphic units present in both wells (Fig. 3).

The Cenozoic fill of the Trujillo Basin ranges in thickness between 3.5 and 11 km and is mainly composed of lower Eocene to Upper Miocene sedimentary rocks (Figs. 2 and 3) as evidenced from the Delfin 1X well (Ibaraki, 1990; Schrader and Cruzado, 1990; Wine et al., 2001; Sternbach et al., 2010). Most of the thick Eocene section of the Trujillo Basin pinches out eastward on the OSH relief (PARSEP, 2001b; Romero et al., 2013) (Figs. 2 and 3). This interpretation is corroborated by seismic mapping of the Eocene onlap, which reveals significant westward expansion of the Eocene section within the basin and limited eastward extension into the Salaverry Basin (Figs. 2-4). In contrast to the relatively undeformed Salaverry Basin, the Trujillo Basin is an elongated, narrow depocenter (~35 km wide), bounded by normal faults and partially inverted during the Neogene (PARSEP, 2001b; Sternbach et al., 2010; Prudhomme et al., 2019) (Fig. 2). Basement normal faulting generated structural highs within the Salaverry basin (Figs. 4 and 5), which, in features such as the Chan Chan High discussed in detail below, played a key role in the formation of structural traps. The incision and fill of trench-orthogonal submarine canyon systems along the steep western side of the OSH indicates a significant accommodation for the proximal sector of the Trujillo Basin during the Middle Miocene-Pliocene (Azalgara, 1993). Part of the 2 km-thick Middle Miocene-Pliocene section of the Salaverry Basin onlaps the eastern flank of the Trujillo Basin (Figs. 2 and 4). The eastern margin of the Salaverry Basin is defined by onlap onto Mesozoic rocks exposed along the coast (Wine et al., 2001; Lopez-Gamundi, 2014; Timoteo et al., 2018) (Fig. 2).

Direct hydrocarbon indicators (DHIs), potentially of biogenic or thermogenic origin, were reported by Timoteo (2015), Timoteo et al. (2018), and Díaz et al. (2019) for the Salaverry Basin, whereas bright spots, enhanced reflections, and gas chimneys were identified by Timoteo (2015). Valencia and Romero (2011) modeled present-day oil and gas generation and expulsion in cases involving thermogenically generated gas. Exploratory efforts have focused on the identification of structural, combined (structural-stratigraphic), and stratigraphic traps in the Miocene section (Valencia et al., 2013), assessing the source rock potential of the Cretaceous section (Timoteo, 2013; Timoteo and Valencia, 2014), and evaluating possible fractured reservoirs in the Mesozoic section (Llerena et al., 2013; Llerena, 2014).

One of the most significant differences between the northern offshore basins of Peru (e.g., the Talara Basin), which contain thick Eocene successions, and the Salaverry Basin is the limited areal extent of Eocene sediments in the latter. The Ballena 1X, the first offshore exploration well drilled in the southern offshore basins, is located on the OSH at a water depth of 106 m (Figs. 1 to 3). The well reached a gneissic basement (Amotape Formation) at a total depth of 975 m (Azalgara, 1993; CoreLab, 2012) (Figs. 2 and 3). Coarse-grained facies, assigned to the upper Eocene Verdun Formation, have been identified in the basal interval (Fig. 3), although alternative interpretations suggest that the Lower Miocene Heath Formation overlies the basement instead (Schrader and Cruzado, 1990; SAVIA, 2014). The stratigraphic column penetrated by the Ballena 1X well consists primarily of Miocene units (Heath, Montero, and Zapallal formations) and Pliocene deposits of the Miramar Formation (Fig. 3). These rock units comprise fine- to medium-grained sandstones and mudstones deposited in inner neritic to upper bathyal environments (Azalgara, 1993; Fig. 3). The lowermost part of the column is characterized by traction-emplaced, cross-bedded sandstones interpreted as delta front-mouth bars. Distributary channel-mouth bar complexes in the Verdun Formation are arranged in coarsening-upwards successions (1 and 2 in figure 3) in turn overlain by prodelta turbidites (3 and 4 in figure 3) (CoreLab, 2012).

The Delfin 1X, drilled at a water depth of 110 m, was the second well drilled in the region. It was the first exploration well drilled in the Trujillo Basin and reached a basement interpreted as Paleozoic foliated mica schists (Azalgara, 1993) at a total depth of 2,668 m (Fig. 2). In this well the Eocene-Oligocene(?) column thickens to approximately 700 m (Fig. 3). This section consists primarily of interbedded limestone, mudstone and siltstone. The lower Eocene Salina Formation was possibly intersected at ~100 m above the basement (Fig. 3). This unit exhibits porosities exceeding 20% in places and shows gas indications (Minguito et al., 1997; PARSEP, 2001b).

In both wells, a thin stratigraphic interval has been partially assigned to the Early Pliocene (Fig. 3). Further basinward, the ODP 684 well in the eastern Trujillo Basin encountered approximately 50 m of Pliocene claystones and fine-grained sandstones (Suess et al., 1988).

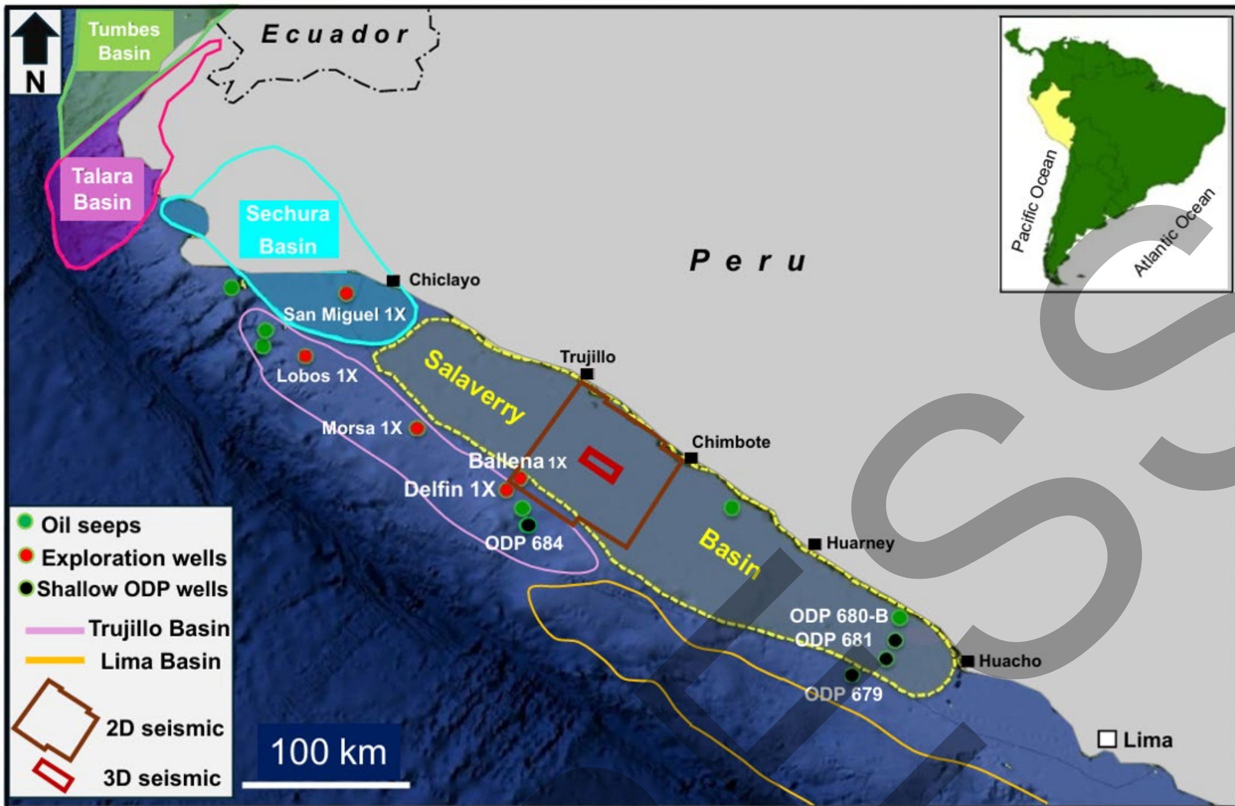

Fig. 1. Map of the forearc basins of northern and central Peru. The oil-producing basins, Talara and Sechura, are located in northernmost Peru and extend both offshore and onshore (Hay-Roe and Miller, 1992; Zuñiga-Rivero et al., 1998; Higley, 2004; Martínez et al., 2005; Fildani et al., 2005; PeruPetro, 2005; Daudt and Scherer, 2006; Meza et al., 2010; Rossello et al., 2022). The Trujillo, Salaverry, and Lima basins lie entirely offshore. This study focuses on the analysis of 2D seismic data (outlined in brown) and the Chan Chan 3D survey (outlined in red) within the central part of the Salaverry Basin (yellow dashed line). Oil seeps and shallow ODP wells are shown as green and black circles, respectively. Modified from Timoteo et al. (2018).

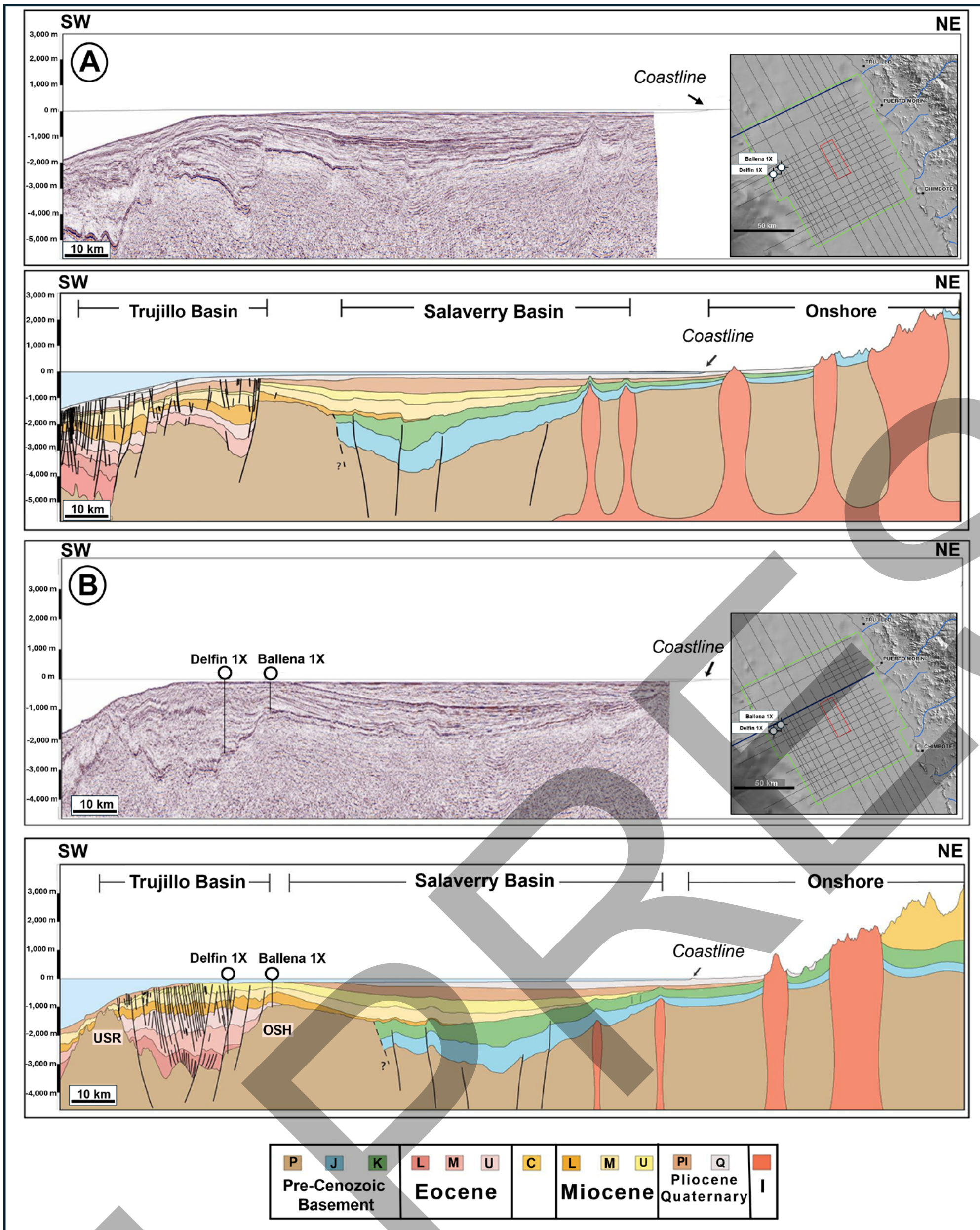

Fig. 2. Seismic stratigraphy of the Trujillo and Salaverry basins: uninterpreted and interpreted. **A.** 2D line 93-45. **B.** 2D line 93-43. Line locations shown as SW-NE black segments on the regional maps. 2D line network in gray, extent of the 2D survey incorporated in the evaluation outlined in green, 3D survey outlined in red. The Trujillo Basin is confined between the Outer Shelf High (OSH) and the Upper Slope Ridge (USR), while the Salaverry Basin is bounded by the OSH to the west and the South American continent to the east. Precambrian and/or Paleozoic basement was encountered in both Delfin 1X and Ballena 1X wells. The strongest reflector across the entire Salaverry and Trujillo basins corresponds to a pre-Cenozoic unconformity (PARSEP 2001a). Note the thick Eocene depocenter in the Trujillo Basin in contrast to the thick Miocene depocenter in the Salaverry Basin. P: Precambrian and/or Paleozoic basement, J: Jurassic, K: Cretaceous, C: Eocene to Miocene, L: Lower, M: Middle, U: Upper, Pl: Pliocene, Q: Quaternary, I: Coastal Batholith. Adapted from Cuipa Vicencio (2018).

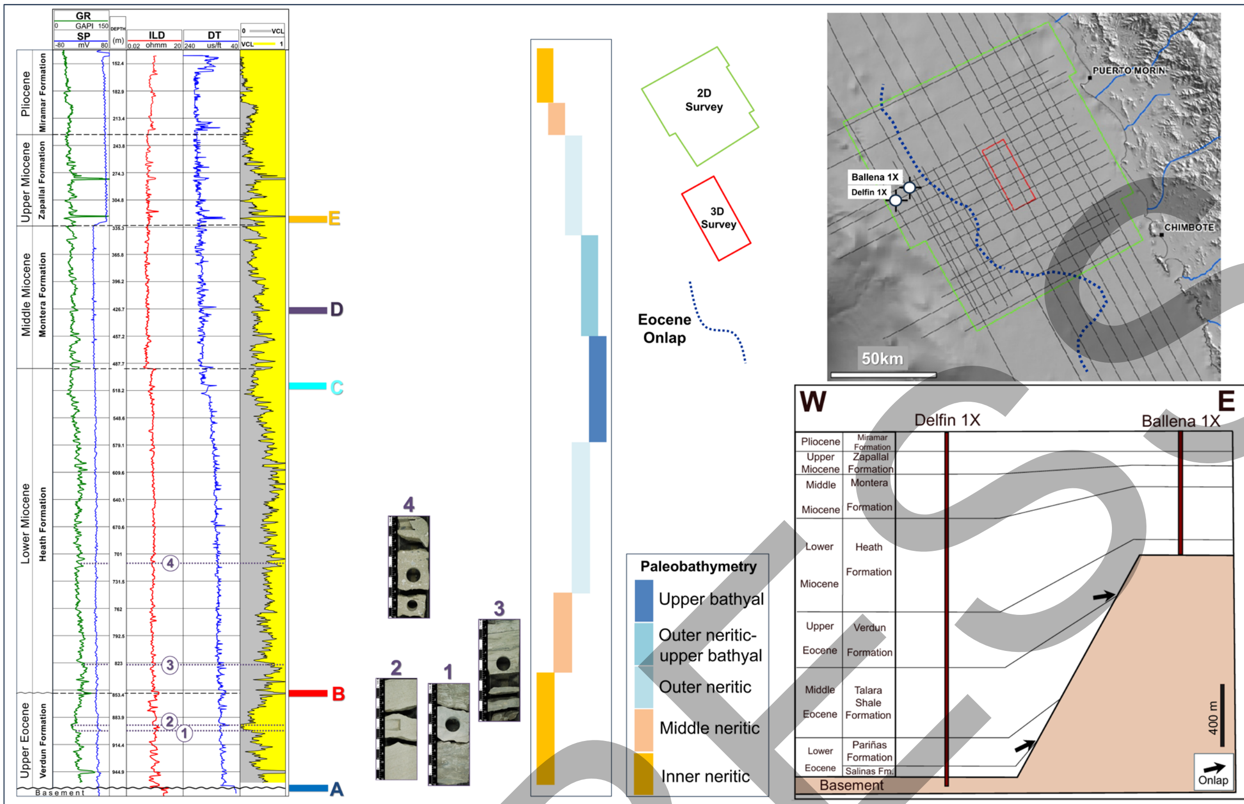

Fig. 3. Trujillo Basin. Ballena 1X well data, adapted from Timoteo (2015) and Timoteo et al. (2018). Well log measurement abbreviations: GR: Gamma Ray (GAPI, Gamma American Petroleum Institute), SP: Spontaneous Potential, ILD: Induction Deep Resistivity, DT: Sonic Transit Time. Color-coded horizontal bars indicate the lower boundary for each depositional sequence (A through E) defined in this study. Note the deepening trend, evidenced by increasing GR, decreasing volume of clay (VCL), and inferred paleobathymetry based on foraminifera (Okada, 1990) and core data analysis. This trend extends from the upper Eocene Verdun Formation through the lower two-thirds of the Lower Miocene Heath Formation. A reversal to a coarsening- and cleaning-upward GR trend (with accompanying decrease in VCL) is observed in the upper third of the Heath Formation and continues through the remainder of the column. The deepening trend reflects a prolonged underfilled stage in the forearc during the Middle and Late Miocene. Eocene onlap mapped on seismic and by well correlation indicates absence of Eocene sediments in the Salaverry Basin. Cores from the Verdun Formation (1, 2) and from the lower half of the Heath Formation (3, 4). 1: Inner shelf-prodelta fine- to medium-grained sandstone; intensely bioturbated mottled interval; original lamination pervasively disturbed. 2: Delta front-mouth; planar cross-bedded sandstone and plant debris. 3: Graded turbidite sandstone beds containing abundant mudclasts at their bases; tops capped by dark, organic-rich claystone. 4: Graded/stratified, locally diffusely cross-bedded pebbly turbidite sandstone. Inset map shows well locations, the 2D lines (gray network), the extent of the 2D survey incorporated in the evaluation (green contour), the extent of the 3D survey (red rectangle), and the inferred position of the Eocene onlap (blue dotted line). Botton right: E-W schematic profile obtained after integrating data from the Ballena 1X and Delfin 1X wells. Core description and interpretation after CoreLab (2012).

3. Methodology

This study is based on an extensive regional 2D seismic grid (two-way travel time, TWT) and a 3D seismic (TWT) survey, the latter covering an area of 364 km^2 in the center of the Salaverry Basin and referred to herein as the Chan Chan survey (Fig. 1). Seismic imaging was generally of good quality; however, resolution and clarity decreased toward the western basin margin, where both shallow and deep direct hydrocarbon indicators have been documented (Timoteo, 2015). Well control is limited to two exploratory wells drilled in 1971 (Ballena 1X and Delfin 1X) and to ODP penetrations farther west in the Trujillo Basin (Fig. 1).

A series of reliable regional horizons served as guidance for the seismic analysis. This allowed the recognition of megasequences, which reflect major episodes of basin and paleogeographic development and are associated with the dominant tectonic processes operating during, or immediately preceding, deposition (Steel, 1993; Paton et al., 2008; Aitken et al., 2011; Paquet et al., 2011; Rouillard et al., 2015; Stewart, 2020). The criterion used to segregate the sedimentary fill into megasequences is typically based on the vertical evolution of three fill stages: underfilled, balanced, and overfilled (Dickinson, 1995; Neal and Abreu, 2009). These megasequences were further subdivided into basin-scale kinetic or kinematic sequences, defined here as sequences limited by unconformities or their correlative syn-deformation conformities. Originally, sequences were defined by Giles and Lawton (2002) in the context of syn-kinematic deposition associated with salt diapirism (halokinetic sequences). These were described as *"relatively conformable successions of growth strata genetically influenced by near surface or extrusive salt movement and are locally bounded at the top and base by angular unconformities that become disconformable to conformable with increasing* *distance from the diapir."* Over time, this concept broadened to encompass any growth or syn-tectonic strata deposited during active deformation. The formation of these sequences may occur due to tectonically or gravity-driven extensional or compressional deformation in a variety of tectonic settings (Horton et al., 2002; Childs et al., 2003; Morley, 2009; Giles, 2010; Maloney et al., 2010; Giles and Rowan, 2012; Lewis et al., 2015; Jolly et al., 2016; Butler, 2019; Coleman et al., 2019). Stratal terminations, particularly angular truncations and onlaps, are critical for the identification of such sequences.

The concept of tectonically related megasequences (*sensu* Williams, 1983) or tectonostratigraphic megasequences (Hubbard et al., 1985; Hubbard, 1988), was applied here to refer to large-scale sedimentary packages deposited during distinct phases of basin evolution. The Miocene-Pliocene fill of the Salaverry Basin was therefore divided into three megasequences labeled in ascending stratigraphic order R, S, and C-MTC (Fig. 4). Each megasequence was characterized based on stratal terminations (Mitchum et al., 1977; Vail et al., 1977) and seismic facies interpretations (Sangree and Widmier, 1977). Four principal stratal terminations (angular truncation, onlap, downlap, and toplap; Mitchum et al.,1977) were used in this analysis. The term baselap was used when terminations of reflectors were difficult to distinguish between original onlap and true depositional downlap rotated by subsequent deformation. These megasequences were further discriminated by subdividing them into kinematic sequences (Fig. 4). The study of these individual sequences was based on stratal terminations, characterization of seismic facies, and identification of geobodies with the help of amplitude maps. The focus on discerning the different kinematic sequences related to the presence or absence of the OSH as a bathymetric high during sedimentation, and, hence to its potential as a source of material in addition to the eastern margin of the basin. Isochore maps were generated for a specific sequence, representing the true vertical thickness (TVD) between two mapped horizons. Thickness was measured vertically from a point on the upper surface to the corresponding point on the lower surface.

As part of the main objective of this study, emphasis was placed on determining the key sand-prone intervals, their characteristics (e.g., depositional environment, areal extent, geometries), and delimitation of potential pathways. Sand detection was conducted with the use of amplitude extractions. RMS (Root-mean-square) amplitude was used here because high values often correlate with the presence of sand due to its higher energy and porosity compared to surrounding rocks (Bacon et al., 2003). RMS amplitude was quantified, mapped, and contoured. Horizon and "gated" amplitude extraction with variable windows were used. A semiquantitative approach, known as A/B ratio, was employed to contrast the amplitude of certain seismic facies (A) versus the "background" amplitude (B). Amplitude attribute analysis was applied to delineate sand fairways and characterize depositional elements. A/B amplitude ratio maps were used as a proxy for relative sand content, capturing variations in seismic waveform asymmetry associated with lithological contrasts between sand- and shale-prone facies. The maximum thickness of the sand-prone intervals was estimated by time-depth conversion.

The underfilled, balanced, and overfilled basin-filling conditions introduced above (Allen and Allen, 2013; Noda, 2016) describe the relationship between accommodation space and sediment supply. An underfilled basin stage develops when the rate of accommodation space creation exceeds sediment supply, resulting in predominantly deep-water depositional conditions. Seismically, it is characterized by thick, relatively uniform, transparent, mud-rich successions containing discontinuous, high-amplitude reflections that represent isolated sand bodies. An overfilled basin stage, on the contrary, develops when sediment supply exceeds the available accommodation space. It is characterized by progressively shallower depositional conditions and basinward-prograding deltaic systems expressed seismically as large, laterally continuous, high-amplitude clinoforms. A balanced basin stage represents an intermediate condition in which sediment supply approximately matches the rate of accommodation creation. Its seismic expression is characterized by high-amplitude, sand-rich bodies that are laterally more continuous than those of underfilled systems but remain separated by seismically transparent, mud-rich intervals.

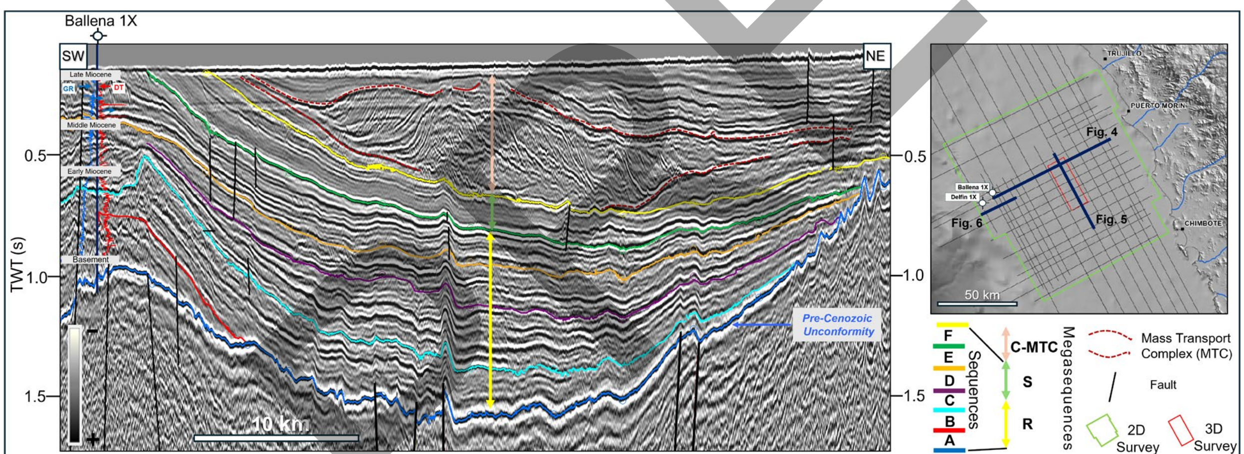

Fig. 4. SW-NE oriented 2D seismic line, showing the three megasequences (R, S, C-MTC) and sequences (A-F) delimited in this contribution. Scale bar indicates the polarity of seismic data. Note gravity-driven deformation (Mass Transport Complex, MTC) in megasequence C-MTC. Clinoforms indicate progradation from the OSH at the base of sequence E. Faults (black lines) appear vertical due to profile exaggeration. Inset map shows well locations, the 2D seismic network (gray lines), the 2D survey area (green contour), the 3D survey area (red rectangle), and the seismic lines depicted in this figure as well as in figures 5 and 6 (blue thick lines). TWT: two-way travel time. GR: Gamma Ray (blue line). DT: Sonic Transit Time (red line). See text for discussion.

4. Results

4.1. Megasequences

Based on seismic facies characteristics, the Miocene-Pliocene basin fill was subdivided into three megasequences: R, S, and C-MTC. Megasequence R shows localized, high-amplitude anomalies associated with isolated channels, terminal splays, and shelf sands interbedded with transparent seismic facies. This megasequence is interpreted to represent a balanced stage, during which accommodation space and sediment supply were approximately in equilibrium. In contrast, Megasequence S represents an underfilled stage and is dominated by transparent seismic facies, indicating that accommodation space exceeded sediment supply. Megasequence C-MTC records the final overfilled stage of basin evolution dominated by abundant sediment supply that exceeded the available accommodation space. Detailed descriptions of these megasequences are provided below.

Megasequence R: It includes sequences B through E. The sequence A, which is restricted to the westernmost sector of the Salaverry Basin, was segregated from this megasequence since it is genetically associated with the Trujillo Basin (Fig. 3). This basinwide megasequence rests on the pre-Cenozoic unconformity and is characterized by moderate to high amplitude, parallel to discontinuous seismic facies. These facies suggest alternating conditions of background sedimentation by settling of sand and finer-sized material. The sequences tend to show progressive onlap along the eastern basin margin while truncation or onlap terminations against the OSH are common on the western margin, with few sequences showing discrete basinward progradational clinoforms off the OSH (Fig. 4). Several sand fairways are identified for this megasequence (see below).

Megasequence S: This megasequence corresponds to sequence F (Fig. 4). Its boundaries coincide with peak transgression in the basin. It is characterized by transparent seismic facies exhibiting high continuity and parallel to sub-parallel low amplitude reflectors. The transparent, parallel nature of the dominant seismic facies in this megasequence suggests background sedimentation by settling of fine material. The reflectors slightly diverge with increasing thickness toward the western margin of the basin. They converge toward the eastern margin, where they lap onto the basement (Fig. 4). In a basin center position two channel-levee complexes: Northern and Chan Chan, rest on the lower megasequence boundary. These complexes exhibit a flat convex or mounded geometry, with alternating low and high amplitude reflections. The detailed seismic characteristics of these complexes are discussed below.

Megasequence C-MTC: Not considered in detail in this study, this megasequence is confined to the center of the basin and represents the peak retrogradation. It is characterized by large clinoforms (C) with associated mass transport complexes (MTC). Azalgara (1993) described the Late Miocene(?)-Pliocene progradation as part of his P sequence, deposited in a shallow basin east of the Salaverry-Trujillo High and interpreted it as a northerly prograding fluviodeltaic system. Timoteo et al. (2018) assigned this megasequence to the Late Pliocene (upper section of the Miramar Formation) and to the Early Pleistocene (Hornillos Formation). The clinoform shoreline trajectory of the combined deltaic pulses shows a progradation of approximately 20 km (Fig. 5). The most common cross-sectional shape for the clinoforms is oblique-progradational (Gong et al., 2015). Asymmetrical, concave-upward clinoforms have been also documented (seismic facies 8 of Timoteo et al., 2018). In dip view, they appear as moderate- to high-amplitude, continuous reflections with wedge-shaped geometries (Fig. 5). In strike view, they appear as mounded features with internal bidirectional downlapping reflections (Fig. 4). The clinoforms are fronted by large-scale mass transport systems characterized by discontinuous to chaotic seismic facies (Fig. 4). Three distinct growth phases of progradation have been identified (Fig. 5) forming “compound clinoform” systems (*cf.* Patruno and Helland-Hansen, 2018). The maximum thickness of the clinoform complex is approximately 500 ms TWT (~429 m), which is similar to the value estimated by Timoteo et al. (2018). These dimensions suggest the presence of shelf edge clinoform sets (Helland-Hansen and Gjelberg, 2012; Patruno and Helland-Hansen, 2018).

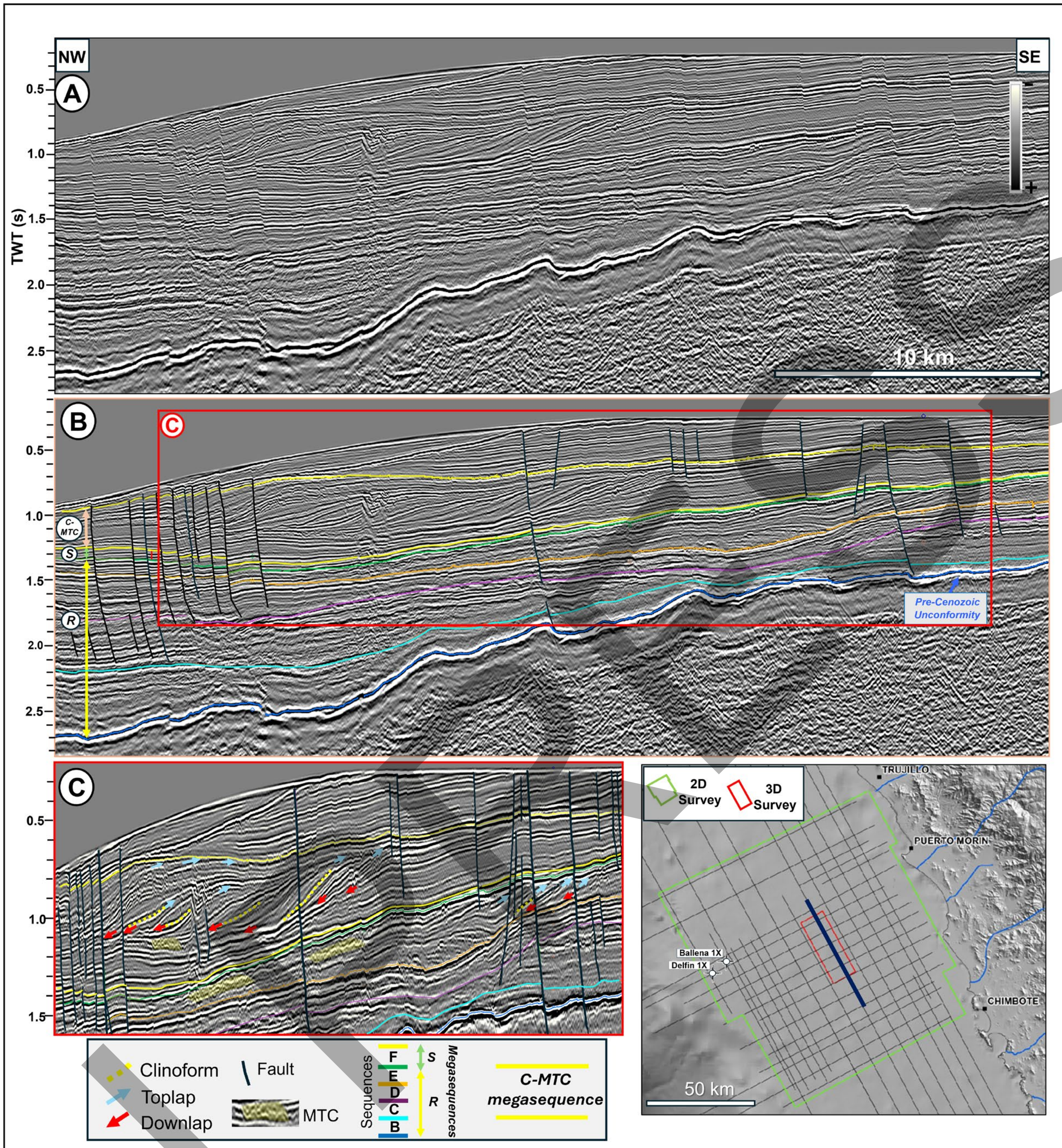

Fig. 5. NW-SE oriented uninterpreted (**A**) and interpreted (**B**) depositional dip cross section of the C-MTC megasequence. Scale bar indicates the polarity of seismic data. Sequences B-E are part of the megasequence R. The S megasequence (=sequence F, see figure 4), characterized by transparent seismic facies, underlies the deltaic clinoforms. **C.** Significantly vertically exaggerated detail shows downlap (red arrows) and toplap (light blue arrows) stratal terminations in the C-MTC megasequence; clinoforms (yellow segmented lines) show at least three distinct growth phases. Note also smaller-scale clinoforms with associated MTC deposits (yellow domains) at their toes in sequence E. Inset map shows well locations, the seismic line depicted in this figure (blue thick line), as well as the 2D seismic network (gray lines), the extent of the 2D survey area (green contour), and the 3D survey area (red rectangle). TWT: two-way travel time. See text for discussion.

4.2. Sequence analysis

This section focuses on the stratigraphic characteristics of sequences A through F, giving attention to the stratal terminations that define each sequence. These are detailed below.

Sequence A (which is part of the Trujillo Basin) is restricted to the westernmost part of the basin. Its eastward termination (Figs. 4 and 6) is interpreted as a baselap, an onlap surface subsequently rotated by tectonic uplift of the OSH. The basal section of the Ballena 1X well correlates with this sequence, likely representing upper Eocene deposits that thicken westward (Figs. 2 and 3). This sequence reflects spatially limited sedimentation in the Salaverry Basin, which was largely exposed to the east, in contrast to the thick Eocene successions developed in the Trujillo Basin (Figs. 2 and 3).

Sequences B-F are fully developed across the Salaverry Basin (Fig. 4). Their varied westward terminations illustrate the episodic tectonic activity of the OSH and uplift and inversion of the Trujillo Basin (Prudhomme et al., 2019). The degree of truncation along the western basin margin decreases progressively from sequence B to sequence D. Significant angular truncation of sequence B along the OSH indicates major uplift and erosion of this tectonic structure (Figs. 4 and 6). Sequence C is partially eroded in some areas but more commonly onlaps along the OSH (Figs. 4 and 6), as well as along the eastern margin (Fig. 4). Sequence D thins and drapes over the OSH, with its depocenter located in the central part of the basin (Figs. 4 and 6). Onlap is common at the base of sequence D against the OSH, whereas in the upper half of this same sequence, eastward (basinward) clinoform progradation with flat toplap surfaces on the eastern side of the

OSH (Fig. 6) indicate wave-base scour in shallow waters. Sequence E is internally dominated by low- to moderate-amplitude reflections exhibiting a broad, regionally divergent pattern toward the west, consistent with the overall westward thickening of the sequence (Fig. 4). Local clinoform progradation off the OSH (Fig. 6) suggests limited accommodation. Sequence F displays a more marked westward-divergent pattern but is characterized by predominantly transparent seismic facies, indicative of significant basin flooding and deposition characterized by settling of fine material. The subsequent truncation of this sequence is attributed to the late-stage uplift of the OSH. Seafloor erosional surfaces caused by strong bottom currents provide evidence of ongoing tectonic uplift (Calvès et al., 2017). The uplift reduced the areal extent of the basin and led to the present configuration represented by the megasequence C-MTC.

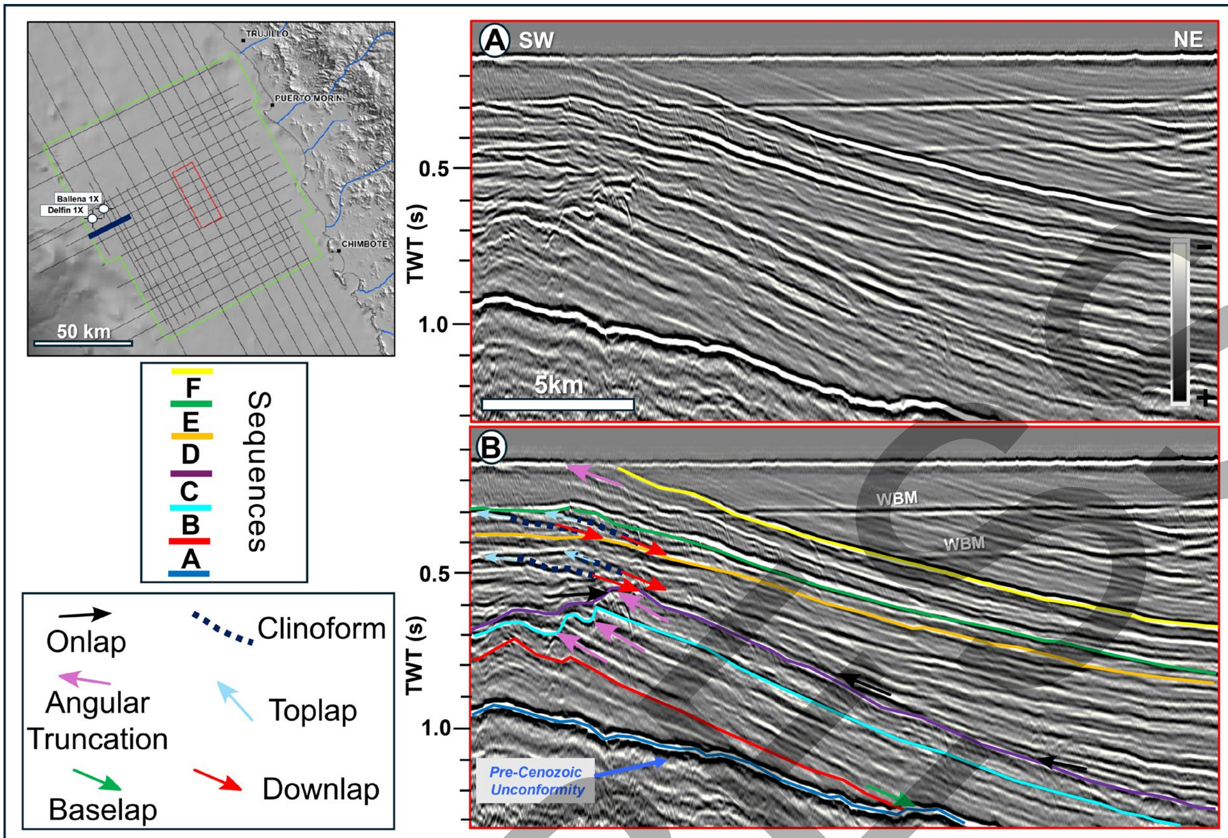

Fig. 6. Stratal terminations along the OSH. Scale bar indicates the polarity of seismic data. **A-B.** Uninterpreted and interpreted SW-NE oriented sections on west margin of the basin. Sequence A (which is part of the Trujillo Basin) thins towards the east as it overlaps pre-Cenozoic basement and thickens westward, suggesting that the OSH was not a positive feature during deposition. Significant erosion of sequences B and C across the OSH indicates major tectonic uplift of this structure. Note onlap at the base of sequence D against the OSH and eastward (basinward) clinoform progradation on the eastern side of the OSH for the upper half of this same sequence. Sequence E shows also basinward progradation evinced by local clinoforms. Note the westward thickening of sequence F with transparent seismic facies and truncation consequence of the late-stage uplift of the OSH. Inset map shows well locations, the seismic line depicted in this figure (blue thick line), as well as the 2D seismic network (gray lines), the extent of the 2D survey area (green contour), and the 3D survey area (red rectangle). WBM: water-bottom multiple, generated when seismic waves reflect off the water surface and the seabed. TWT: two-way travel time. See text for discussion.

The isochore map of sequence C illustrates coastal (eastward) and distal (westward) onlap terminations (Fig. 7). The stratal terminations of sequences B and D-F along the eastward (landward) basin margin are characterized by progressive onlaps as well (Fig. 8A). Isochore maps of sequences B and D also terminate in onlaps onto the coastal basin margin (Fig. 8B, C). The systematic thinning of all these sequences against the costal margin, along with the landward progression of onlaps onto the inherited topography, indicates an increase in coastal accommodation space (Fig. 8A).

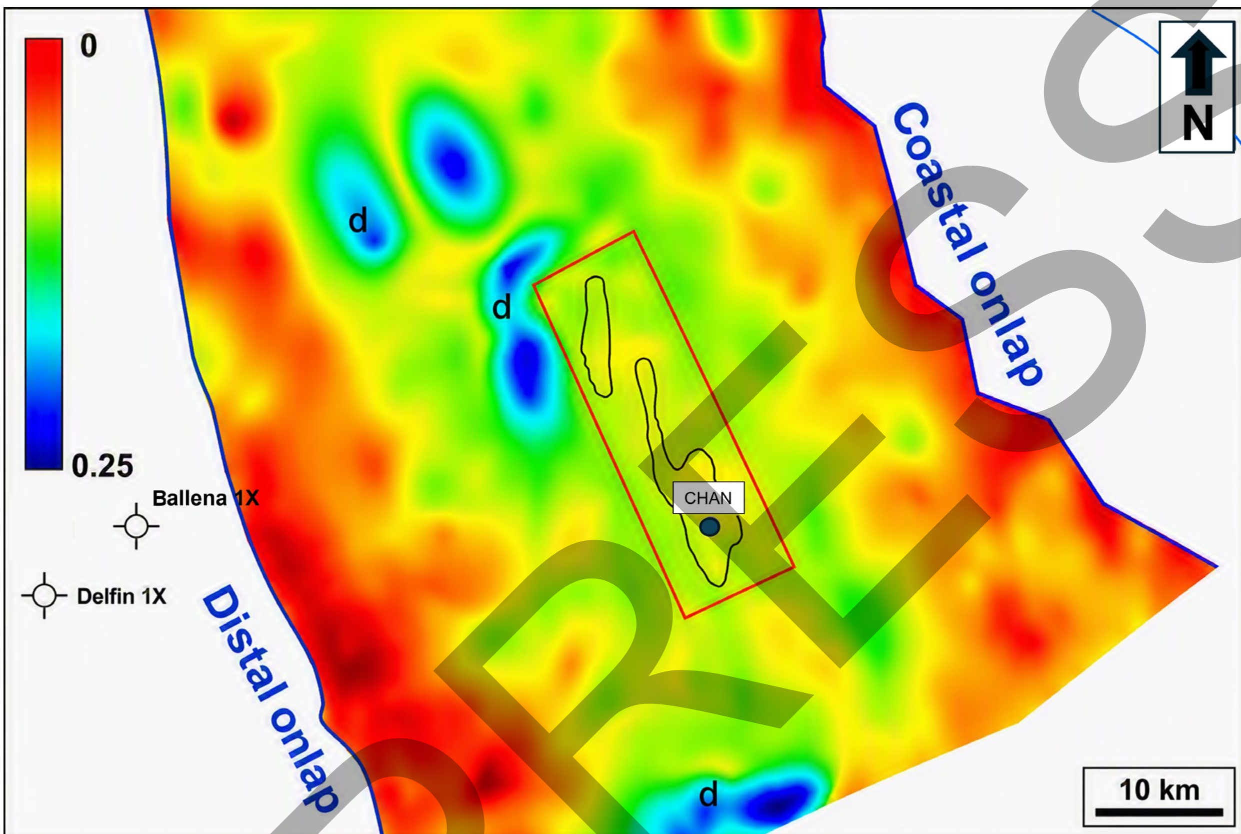

Fig. 7. Isochore map (in seconds) of sequence C. Three minor depocenters (cool-colored areas, labelled "d") are evident towards the center of the basin. Coastal onlap along the eastern (landward) basin margin is noticed by gradual decrease of isochron values approaching zero, while distant (seaward) onlap on the OSH is similarly indicated by isochores thinning to zero. Black-outlined areas within the 3D survey footprint (red rectangle) highlight potential stratigraphic and structural traps associated with the North and Chan Chan channel-levee complexes of sequence F. CHAN denotes the location of a potential vertical exploration well targeting the Chan Chan trap. See text for discussion.

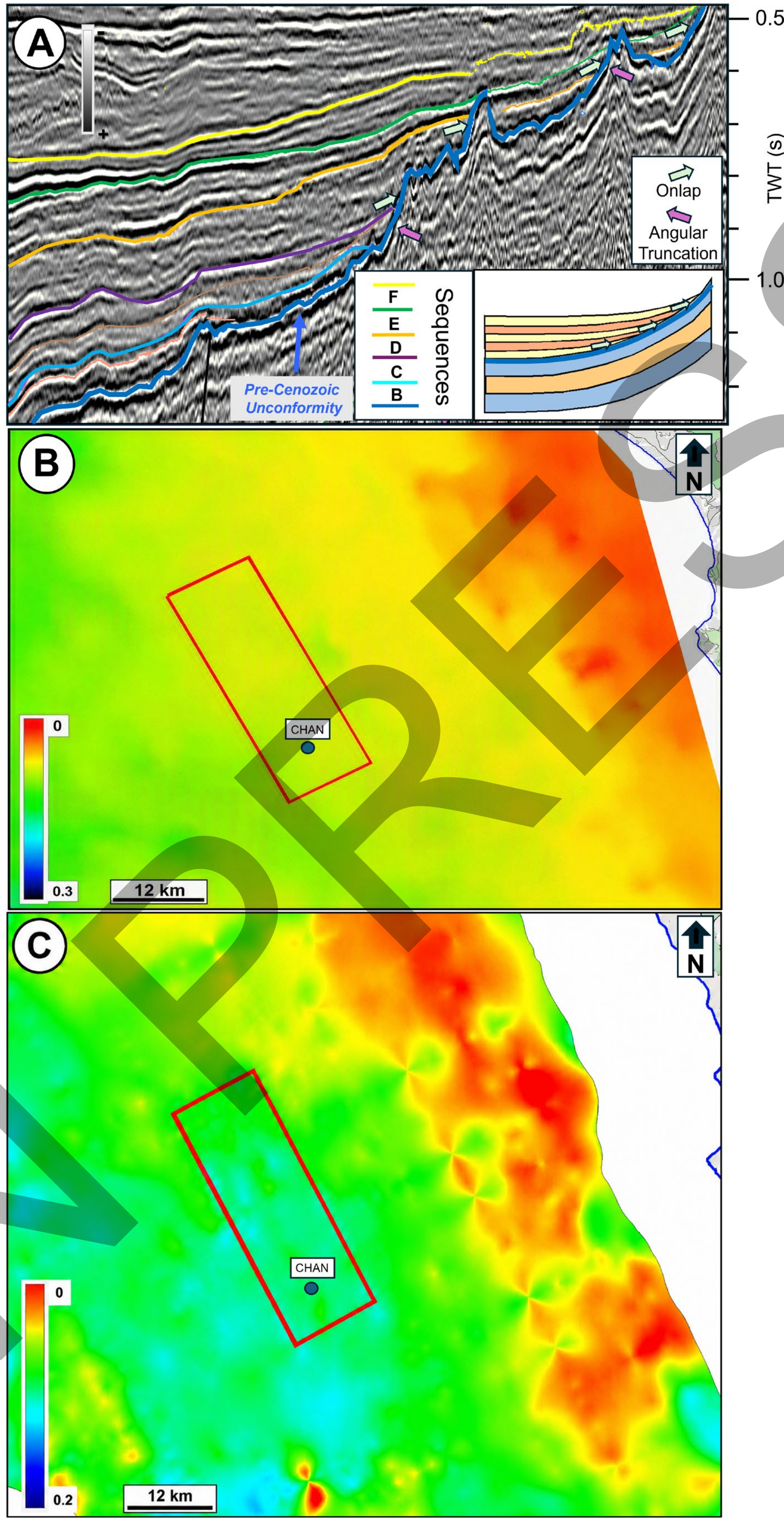

A
0.5
1.0
TWT (s)
Onlap
Angular Truncation
Pre-Cenozoic Unconformity
F
E
D
C
B
Sequences
B
N
CHAN
0
0.3
12 km
C
N
CHAN
0
0.2
12 km

Fig. 8. Stratal terminations along the eastern basin margin. Scale bar indicates the polarity of seismic data. **A.** Coastal onlap of sequences B-F highlights progressive eastward basin expansion (see scheme). Thinning towards the east, especially for sequences B and E, indicates periods of maximum subsidence. Orange thin lines represent intra-sequence horizons, which also show progressive onlap. **B.** Isochore map (in seconds) of sequence B. The landward extent of the isochore is extrapolated beyond the limits of the 2D seismic lines. **C.** Isochore map (in seconds) of sequence D. The coastal onlap of this sequence extends farther landward when compared to the onlap of sequence C (see figure 7); however, due to poor seismic quality, this onlap is not fully captured in the isochore map. Note the smooth eastward thinning of sequence B and the uneven thinning of sequence D due to basement highs. Outline of 3D survey in red. TWT: two-way travel time. CHAN denotes the location of a potential vertical exploration well targeting the Chan Chan trap. See text for details.

4.3. Sand fairways

Sand sediments are transported through forearc basins either transverse to basin trend across shelves or slopes or along the basin axis (Dickinson and Seely, 1979; Noda 2016). Analysis based on gated RMS amplitudes and identification of seismic facies helped map sand-rich intervals in sequences B-F. Due to the low to moderate resolution of the 3D volume, with a dominant frequency of around 30 Hz, identification of seismic facies was challenging when the sand-prone intervals were thin and lateral changes were subtle. The principal sand complexes are described below in ascending stratigraphic order.

4.3.1. Sequence B

Basal Sand Complex

Identified in the lower half of sequence B, this reflection is characterized by a high amplitude that produces a strong response in the amplitude maps (Fig. 9A), especially over and on the southern flank of the Chan Chan High. To the north of the high, it nearly blends into the background amplitude signal (Fig. 9A). Its distribution within the Chan Chan 3D survey suggests that the anomaly continues southward, into an area where only a regional 2D grid is available (Fig. 9A).

Three lines help illustrate the nature of this sand complex and its interaction with the Chan Chan High (Fig. 9B-D). The dip lines (Fig. 9C, D) reveal a clear brightening of the amplitudes over and south of the high, consistent with the amplitude response observed in the map (Fig. 9A). Additionally, there is a noticeable thickening trend of the entire basal section on both flanks of the high, suggesting a syn-depositional growth rather than a simple buttressing effect. These thickening and thinning trends differ in the strike direction where, although the thinnest section also rests on top of this high, there is a moderate to low increase in thickness relative to the crest on the southern flank and a much-pronounced thickening on the northern flank, the latter also accompanied by amplitude dimming (Fig. 9B). Sand presence was assessed semiquantitatively by applying an A/B amplitude ratio methodology. A/B values in the sand complex ranging from around 3 to ~4.3 are indicative of improved sand development.

Transgressive sands, typically thin deposits formed by shoreface retreat or barrier in-place drowning (Cattaneo and Steel, 2003), are proposed as the depositional model for the Basal Sand Complex. Transparent seismic facies, interpreted as mud-rich deposits, surround and blanket this complex. Such transgressive sandy deposits are commonly overlain by fine-grained offshore or shelf sediments during the transition from shoreface sands to muds in the late stages of transgression (Demarest and Kraft, 1987; Nummedal and Swift, 1987; Reinson, 1992; Clifton, 2006; Lee et al., 2020). The basal section shows a clear progressive onlap configuration. Its presence, albeit thinner, over the Chan Chan High suggests a balance between accommodation rate, controlled by uplift/subsidence, and supply rate. The thickening of the section and the dimming of the amplitude away from the high indicate reduced accommodation space on the high, favoring reworking and subsequent deposition of transgressive sands. This interpretation is supported by amplitude maps (Fig. 9A) and seismic sections (Fig. 9B-D). Furthermore, the dimming and conspicuous absence of high amplitudes of the basal section north of the high (Fig. 9A) suggests sedimentation dominated by settling fines. Under these accommodation/supply conditions, depositional scenarios 2 and 3, outlined in figure 10, are most applicable. These scenarios result in either discontinuous transgressive sands (Scenario 2) or blanket-like transgressive sands (Scenario 3), with facies successions that may include fluvial deposits at the base (if preserved), overlain by foreshore and shoreface sands. In contrast, north of the Chan Chan High, rapid transgression and in-place drowning dominated, leading to fine-grained sedimentation and the absence of basal transgressive sands.

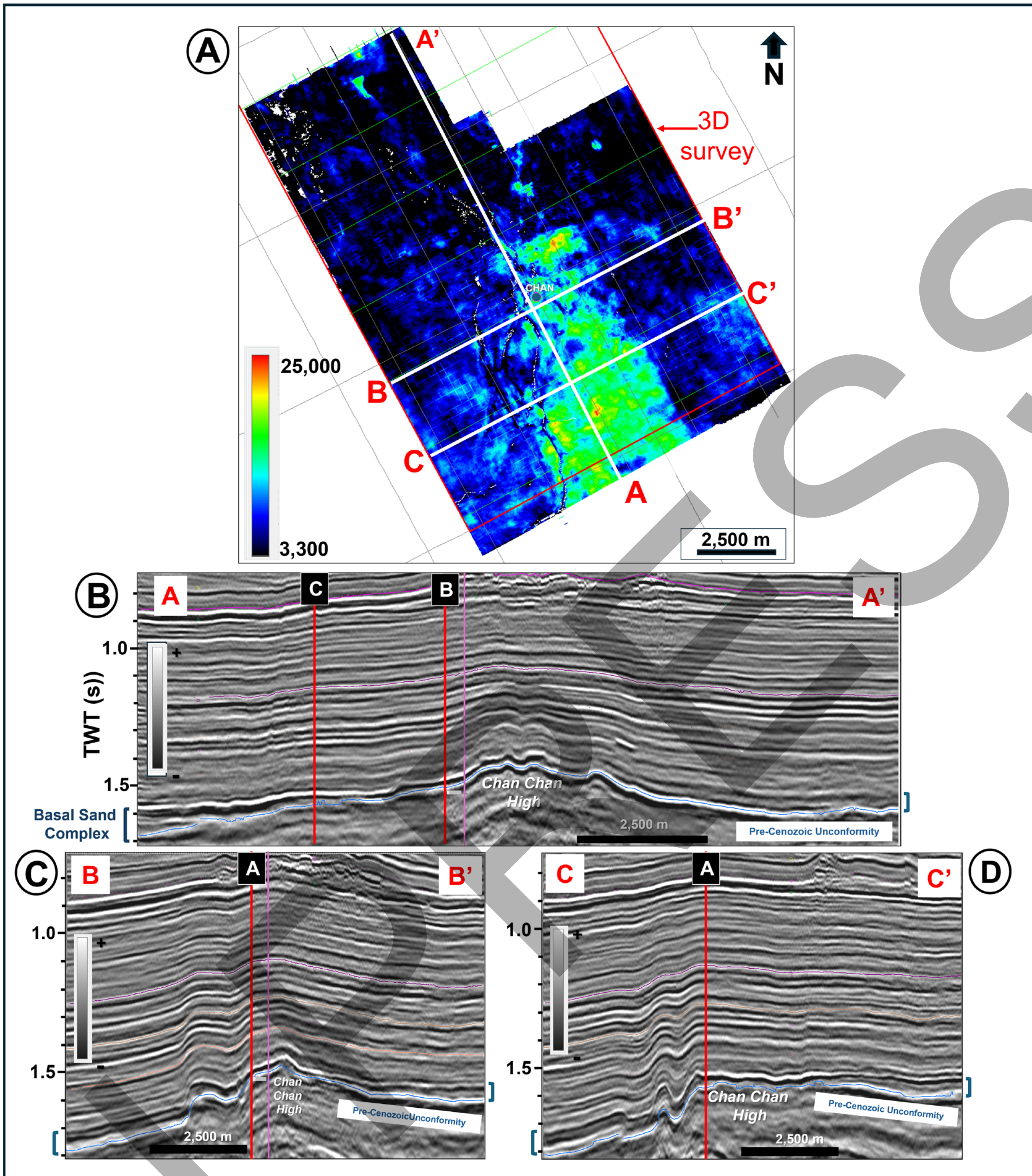

Fig. 9. Basal Sand Complex, sequence B. **A.** Root-mean-square (RMS) map. A "gated' RMS amplitude extraction was performed using variable windows extending from the pre-Cenozoic unconformity to a strong reflection at the top of the complex. High RMS values are shown in warm colors, while low values appear in cool colors. The Chan Chan 3D survey outline is shown in red. The white lines refer to seismic sections shown in panels B to D. 2D seismic network shown as gray lines. Inner grid of the 3D and part of the 2D lines used for amplitude map generation shown as thin, faint lines. **B.** SE-NW section (A-A'): note amplitude dimming north of the Chan Chan High and thickening of the basal section away from it. **C-D.** SW-NE dip sections (B-B' and C-C'): both show amplitude brightening on the Chan Chan High and dimming away from it. The basal interval thickens away from the high. In panels B-D, the red vertical lines refer to the position

of the other seismic profiles. Purple vertical lines in B and C denote the location of a potential vertical exploration well CHAN (see panel A) targeting the Chan Chan trap. Scale bars indicate the polarity of seismic data. TWT: two-way travel time.

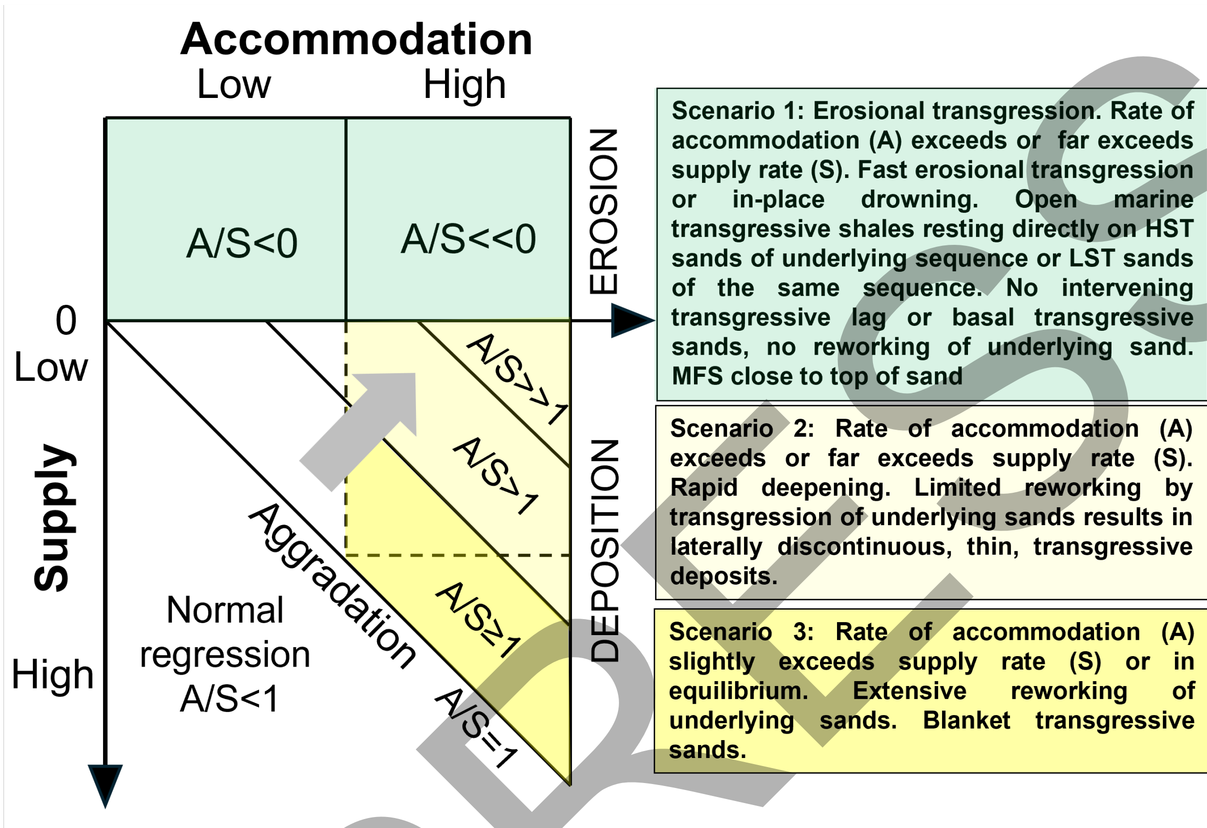

Fig. 10. Depositional models under varying accommodation and sediment supply conditions, after Curray (1964) and Cattaneo and Steel (2003). Transgressive deposits and the preservation of transgressive sands are shown as a function of accommodation rate (A) and sediment supply rate (S). The gray arrow indicates the trend of decreasing sediment supply and increasing accommodation. The Basal Sand Complex is interpreted to have formed during a transitional stage between scenarios 2 and 3. Scenario 3 (blanket transgressive sands) and Scenario 2 (discontinuous transgressive sands) are suggested to prevail south of and on the Chan Chan High. In contrast, Scenario 1, where accommodation rate greatly exceeds supply rate, dominates north of this high, resulting in the absence of transgressive sands and the deposition of fine-grained sediments through suspension settling. HST: highstand systems tract. LST: lowstand systems tract. MFS: maximum flooding surface. See text for details.

High-sinuosity channels

Shoestring elements are visible in the upper half of sequence B on the 3D seismic volume (Fig. 11). These features, labeled 1-3 in figure 11, correspond to channel systems with moderate to high sinuosity (see below). Channels 1 and 2 are part of the same system and are located just below the reference horizon, whereas channel 3 lies slightly above it. Both channel systems, along with the terminal splay or lobe (feature 4 in figure 11A), display A/B amplitude ratios greater than 2, although values are relatively low overall. Nevertheless, their amplitude contrast suggests the presence of sand-prone deposits. A detail of channel 3 is shown in figure 12.

The seismic expression of the channel systems is marked by single-cycle, high-amplitude reflections with limited lateral continuity in the dip direction. In contrast, the terminal splay or lobe (feature 4) exhibits similar seismic characteristics but is substantially more laterally extensive.

Based on their morphology and length-to-width (L/W) ratios, these features are categorized as sinuous channels (sections C through E in figure 12) with L/W ratios of 3 or greater, and as lobes or terminal splays (section F in figure 12) with L/W ratios near 1. Moderate- to high-sinuosity RMS-attribute anomalies, and their associated lobate RMS-attribute features (Fig. 12), are interpreted as feeder channels and their related terminal splays or lobes. (McHargue et al., 2021). Unlike the feeder channels updip (sections C through E in figure 12), the terminal splay/lobe displays a well-defined tabular geometry. It has a cross-sectional width of approximately 2.5 km (section F in figure 12). Paleoflow is inferred to have been transverse to the basin, from NE to SW. Similar updip-downdip transitions from channelized flow to an unconfined frontal splay/lobe have been amply documented in the deep-water literature. (e.g., Posamentier, 2003; Saller et al., 2008; Cross et al., 2009; Oyedele et al., 2015).

The distal segment of channel 1 (and channel 2) shows reduced sinuosity and channel straightening, interpreted as a response to an increase in slope gradient (Babonneau et al., 2002). In contrast, channel 3, which remains relatively straight along its entire length, shows erosion primarily confined to the channel axis (Zulkifli et al., 2024). The channels observed in this interval are relatively thin, with no evidence of significant vertical aggradation (Deptuck et al., 2007; McHargue et al., 2011; Jobe et al., 2016).

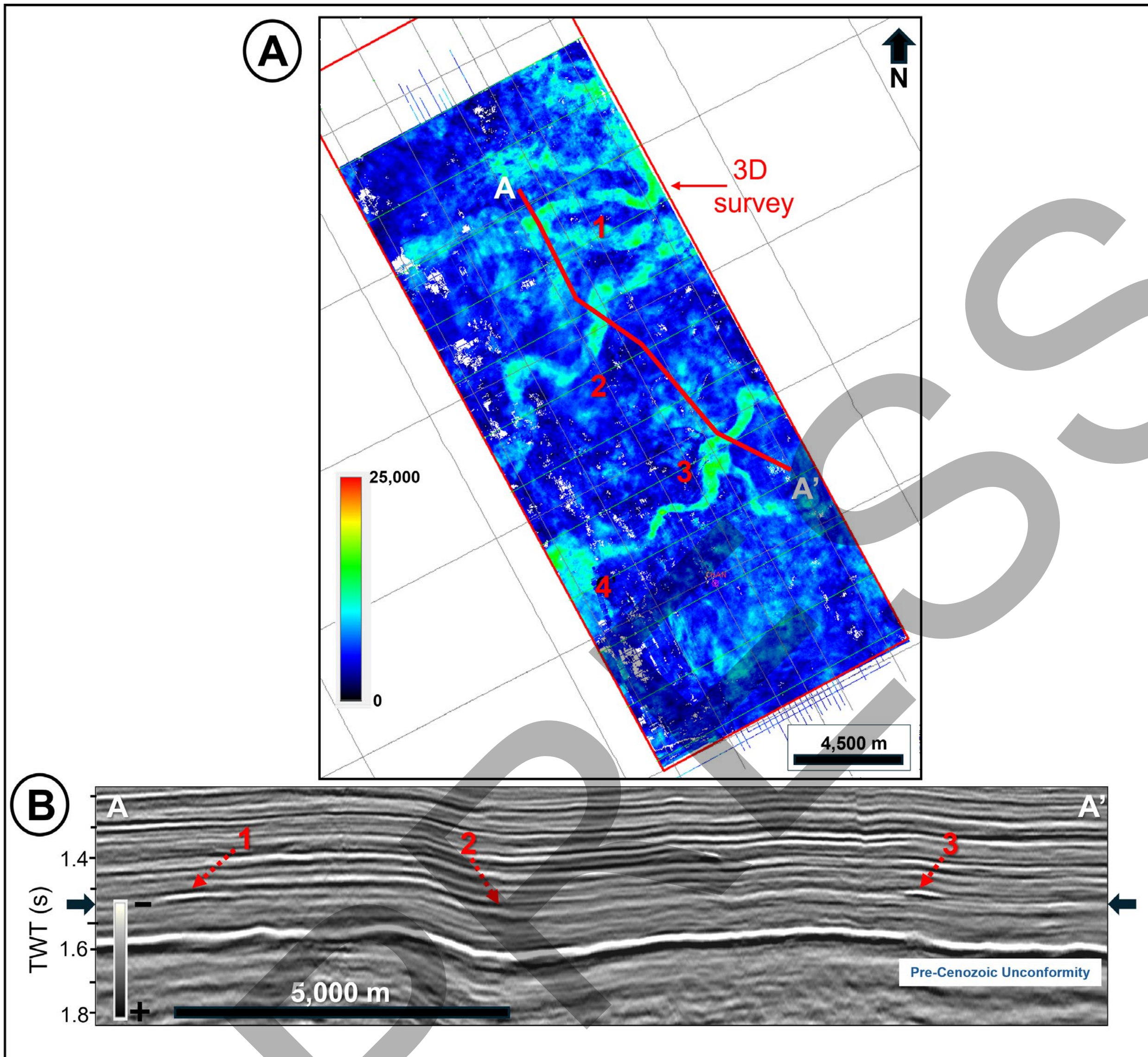

Fig. 11. A. Root-mean-square (RMS) amplitude map of the upper half of sequence B. High RMS values are shown in warm colors, while low values appear in cool colors. The RMS window (-10ms, +30ms) reveals two main channel systems: features 1 and 2, interpreted as segments of a single high-sinuosity system, and feature 3, which appears to terminate in a minor terminal splay or lobe (feature 4 on map). A/B amplitude ratios are relatively low (~2.3) across the channel systems, indicating limited sand development. CHAN denotes the location of a potential vertical exploration well targeting the Chan Chan trap. Outline of the 3D survey in red. 2D seismic network shown as gray lines. Inner grid of the 3D and part of the 2D lines used for amplitude map generation shown as thin, faint lines. **B.** NW-SE oriented A-A' arbitrary line, showing the seismic expression of channels 1-2 and 3. The 1-2 channel system lies just below the reference horizon (black arrows) used in the RMS amplitude map, while channel 3 is slightly above it. Scale bar indicates the polarity of seismic data. TWT: two-way travel time.

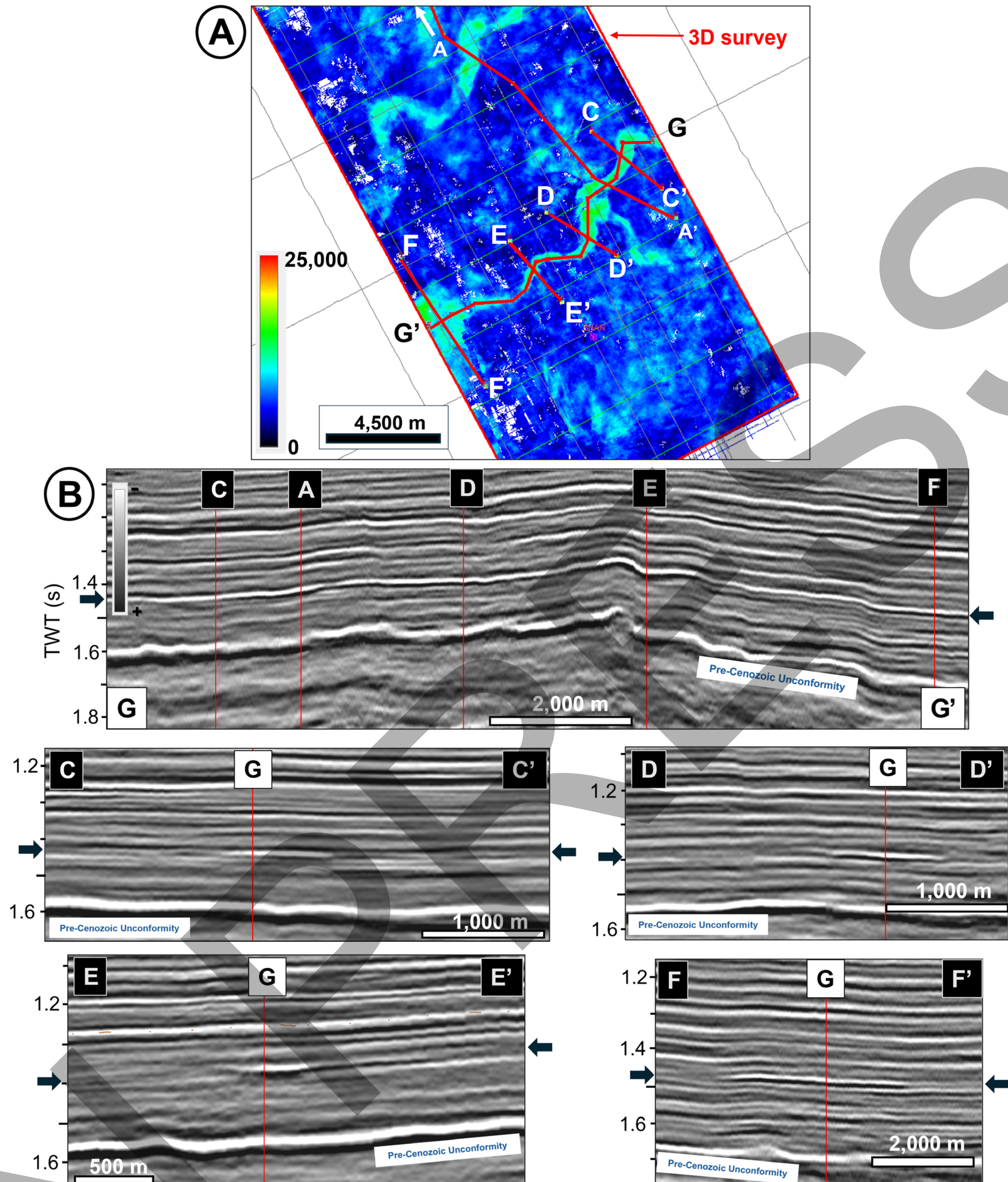

Fig. 12. Detail of channel 3, sequence B (see full map in figure 11A). **A.** Gated (-10ms, +30ms) RMS amplitude map, illustrating the position of the channel and of its lobe features. Profile A-A' shown as reference. High RMS values are shown in warm colors, while low values appear in cool colors. CHAN denotes the location of a potential vertical exploration well targeting the Chan Chan trap. Outline of the 3D survey in red. 2D seismic network shown as gray lines. Inner grid of the 3D and part of the 2D lines used for amplitude map generation shown as thin, faint lines. **B.** NE-SW oriented, dip section along the channel (G-G'), with several NW-SE oriented cross-sectional views of the channel and its terminal splay/lobe. The red vertical lines in G-G' refer to the position of the cross-sectional profiles. Reference horizons shown as

black arrows. Scale bar indicates the polarity of seismic data. TWT: two-way travel time.

Similar seismic facies to those identified in sequence B, though more poorly defined, characterize the sand-prone intervals within sequence C (Fig. 13). RMS amplitude extractions reveal geometries comprising a few narrow, channel-like shoestring forms, with L/W ratios of 3 or greater, and subordinate, large splay-like elements, approximately 2.5-3.5 km in both length and width, exhibiting near-equidimensional (L/W≈1) geometries (Fig. 13). Smaller equidimensional forms, roughly 1 km in size, are interpreted as overbank or spillover lobes (Wynn et al., 2007; Hubbard et al., 2009; Eschard et al., 2013; Kjøll et al., 2025). These sand-rich elements are marked by high-amplitude reflections that contrast sharply with the background seismic character.

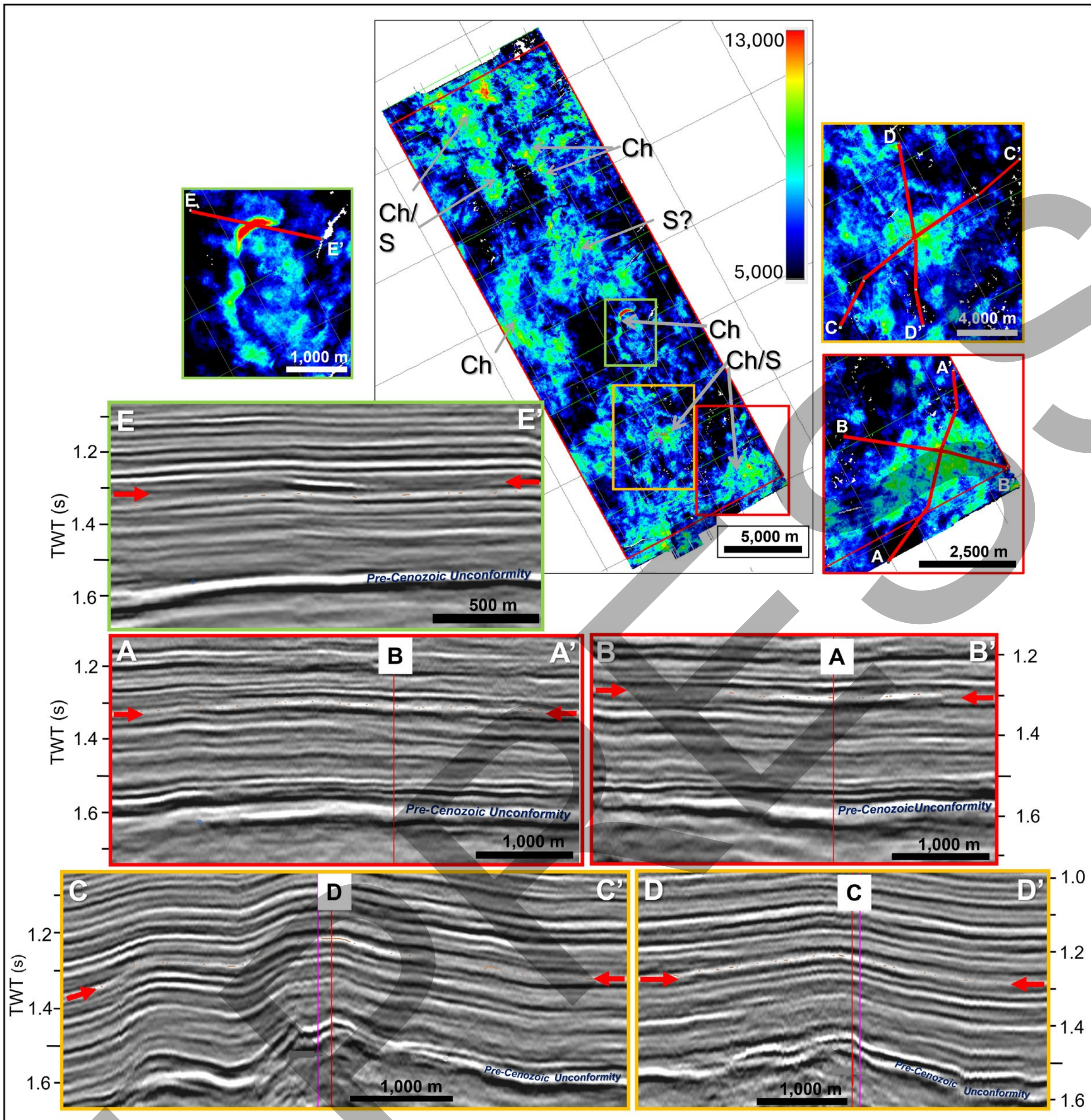

Fig. 13. Root-mean-square (RMS) amplitude map of the depositional elements in sequence C, including splay-like features (S) and channel-like, shoestring forms (Ch). High RMS values are shown in warm colors, while low values appear in cool colors. The 3D survey outline is shown in red, matching the main map. 2D seismic network shown as gray lines. Inner grid of the 3D and part of the 2D lines used for amplitude map generation shown as thin, faint lines. CHAN denotes the proposed location of a vertical exploration well targeting the Chan Chan trap. Squares in the lower half of the map refer to individual panels A-A', B-B', C-C', and D-D', which represent seismic sections of splay-like elements, and panel E-E', which shows a cross-section of channel-like forms (zoomed-in excerpts showing section locations provided next to the main map). The red vertical lines in some profiles indicate the position of the intersecting profiles. Red arrows indicate horizons for gated (0, -40ms) amplitude extraction. The apex of the Chan Chan trap is displayed on seismic lines C-C′ and D-D' by a magenta vertical line. Scale bar as in figure 12B. TWT: two-way travel time.

4.3.2. Sequence E

Isolated shelf(?) sands

In the uppermost section of sequence E, a series of strong reflections were selected for further evaluation due to its areal extent and amplitude strength. The RMS amplitude map (Fig. 14) reveals moderately well-defined bodies with low A/B ratios (≤2), characterized by discontinuous linear to slightly curved amplitudes. The bodies are thin (approximately one seismic cycle), with a ~N-S orientation, and display L/W ratios ranging from 3 to 5 (average: 4.2), with maximum lengths up to 4.5 km (Fig. 14). While linear shelf ridges can occasionally extend tens of km, smaller (<few km) ridges are generally thin (<10 m) and hundreds of meters wide (Swift and Field, 1981; Snedden et al., 1999; Bassetti et al., 2006). Based on their geometry and seismic character, these features are interpreted as outer shelf isolated sand bodies. Their limited thickness and extent suggest deposition under conditions of low accommodation and limited sediment supply during an early transgressive phase (Posamentier, 2002; Cattaneo and Steel, 2003; Suter, 2006; Chiarella et al., 2020).

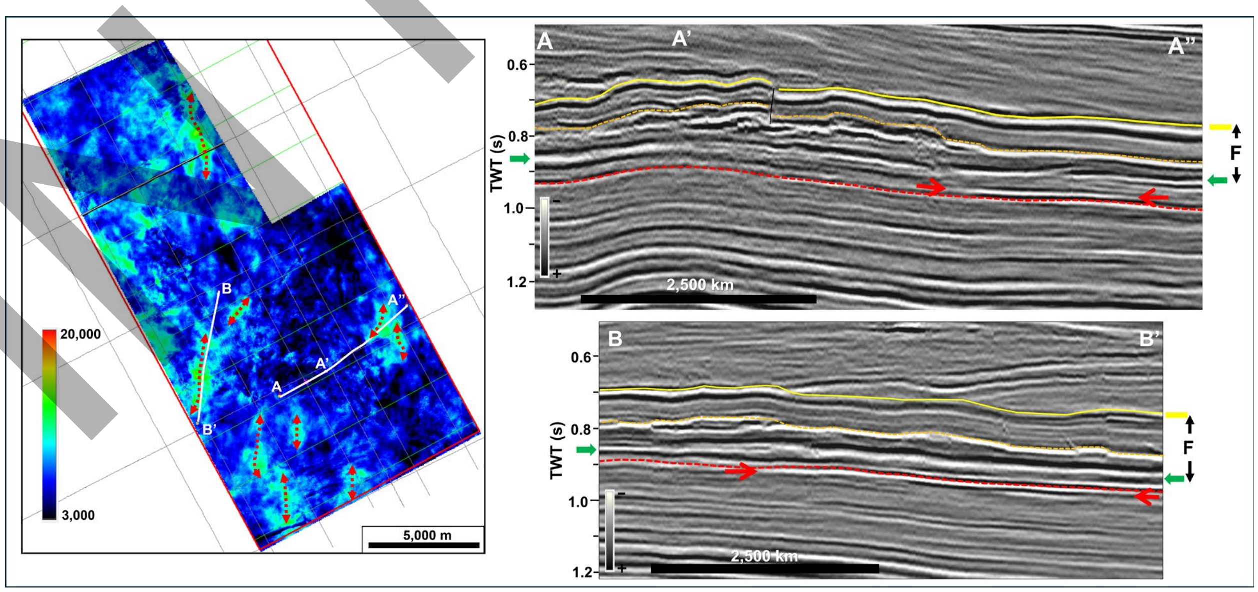

Fig. 14. Root-mean-square (RMS) amplitude map of the uppermost section of sequence E. High RMS values are displayed in warm colors, while low values appear in cool colors. The outline of the 3D survey is shown in red. 2D seismic network shown as gray lines. Inner grid of the 3D and part of the 2D lines used for amplitude map generation shown as thin, faint lines. Purple dot denotes the proposed location of a vertical exploration well targeting the Chan Chan trap. The dashed red lines represent the horizons used to generate the gated (-30ms, +10ms) amplitude map. Green arrows on the seismic cross sections mark the lower boundary of sequence F; the yellow continuous line indicates its upper boundary. Intra-sequence horizon (dashed yellow line) demarks top of mounded geometries in the lower part of said sequence. On the A-A'' arbitrary line, the red arrows highlight the length of a potential sand ridge located immediately above the dashed red horizon, whereas on the B-B′ line, a similar sand ridge locates immediately below this horizon. Scale bar indicates the polarity of seismic data. TWT: two-way travel time.

4.3.3. Sequence F

Channel-levee complexes

Two channel-levee-fan complexes were identified from both 2D seismic lines and the 3D survey (Fig. 15). A channel-levee complex is defined here as a stack of two or more architecturally similar elements with consistent stacking patterns. These features, named here as North Complex and Chan Chan Complex, lie near the center of the basin and rest on the lower boundary of sequence F (Fig. 15). This boundary forms a prominent, regionally mappable seismic horizon. Both complexes are overlain by the dominant transparent seismic facies that characterizes sequence F, and each exhibits positive morphological relief (Fig. 15). The presence of sand-rich channel fills within the core of the complexes results in differential compaction. The North Complex has a maximum thickness of 0.08 s TWT (~89 m). It is thinner than the Chan Chan Complex (see below) and displays a characteristic double downlapping pattern.

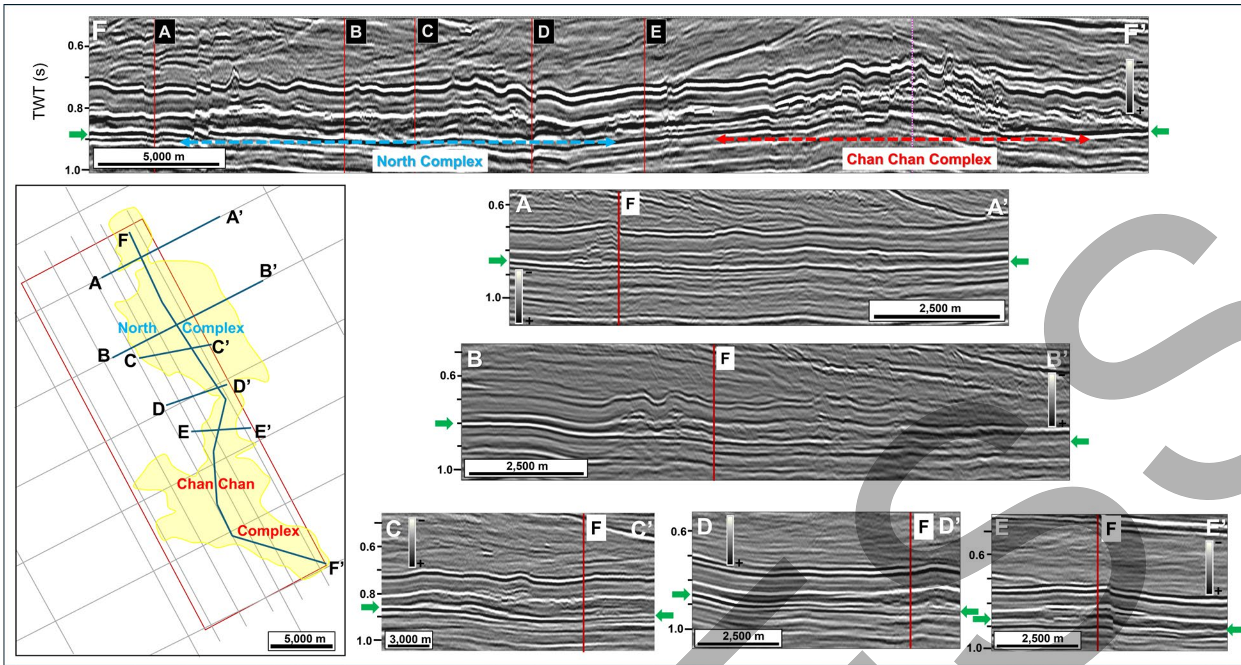

Fig. 15. Channel-levee-fan complexes at the base of sequence F. The outline of the 3D survey is shown in red. 2D seismic network shown as gray lines. Yellow area on map shows the extent of both channel-levee-fan complexes. Green arrows on the seismic cross sections indicate the basal boundary of sequence F, on which both the North and Chan Chan complexes are developed. The A-A' to D-D' lines show the development and internal architecture of the North Complex. The E-E' line illustrates inter-complex facies toward the SSE where the Chan Chan Complex is located. The F-F' arbitrary 3D line along depositional strike depicts the lateral relationship of both complexes. Inferred paleoflow direction is from SE to NW. The red vertical lines in the profiles indicate the position of the intersecting profiles. The apex of the Chan Chan trap is displayed on F-F' by a magenta vertical line. Scale bars indicate the polarity of seismic data. TWT: two-way travel time.

The Chan Chan complex is the largest of the complexes identified. It displays seismic facies similar to those of the North Complex, characterized by high-amplitude, laterally discontinuous reflections (Fig. 15). The complex reaches a maximum thickness of approximately 0.1 s TWT (~106 m) and exhibits a distinct double downlapping configuration, most clearly observed on dip-oriented seismic profiles (Fig. 16), a feature typical of channelized lobate complexes (Heritier et al., 1979; McGovney and Radovich, 1985; Mitchum, 1985; Posamentier and Erskine, 1991; Weimer, 1991). The spatial evolution of the Chan Chan Complex is illustrated along a NW-SE dip-oriented transect

(Fig. 16). In cross section, this complex reveals a pronounced "gull wing" morphology, similar to that observed in the North Complex. This geometry is formed by proximal levees that downlap toward their flanks (Flood et al., 1991; Shew et al., 1993; Babonneau et al., 2002; Fonnesu, 2003; Posamentier and Kolla, 2003; Saller et al., 2004; Qi et al., 2021; Haq et al., 2023). Channel fills (F1 seismic facies in figure 17) are characterized by high-amplitude, laterally discontinuous reflections (high-amplitude reflection packets or HARPs; Flood et al., 1991). Upright stacks of F1 facies units indicate a rather vertical channel migration pattern resulting in a stable aggradational main channel (*cf.* Gervais et al., 2004). Based on their cross-sectional shape and continuous reflections of variable seismic amplitude that converge away from the channel axis, two components of a levee system are identified: proximal and distal (Fig. 17). The F2 seismic facies is defined by discontinuous to semicontinuous reflections that downlap away from the channel axis, divergent toward the channel core (F1 facies) and convergent toward the flanks. This facies is interpreted as representing the proximal or inner levees of the channel-levee system. Laterally, F2 transitions into a thinner F3 seismic facies, characterized by lower amplitudes and greater continuity, likely representing distal or outer levees. This seismic facies association exhibits a cross-sectional external geometry of aggradational channel-levee complex (Catterall et al., 2010). Both the North and Chan Chan complexes are draped by a laterally continuous, low amplitude to transparent seismic facies (FI in figure 17). This facies, which dominates sequence F (Fig. 4), is interpreted as fine-grained sediments deposited by suspension settling. The FI facies thins over the axis of the channel (F1 facies), indicating differential compaction over a sand-rich, bathymetrically elevated channel complex.

The relatively high, mound-like relief of the Chan Chan Complex suggests a mixed mud-sand system, contrasting with sand-rich systems which, although also constructional, tend to exhibit low relief (e.g., Emery and Myers, 1996). These mixed systems typically display moderate to high reservoir heterogeneity, moderate vertical communication, and limited lateral communication. Estimated sand-to-mud ratios range from approximately 30% in the F2 seismic facies to as high as 70% in the F1 facies. The pronounced relief of the mud-sand complex likely contributes to the development of stratigraphic traps via postdepositional differential compaction (Heritier et al., 1979; Brewster, 1991). Positive differential compaction (e.g., Chopra and Marfurt, 2012) occurs when the material within a channel is less compactable than the surrounding lithology, often resulting in the development of inverted topography. Two such potential traps, associated with the North and Chan Chan channel-lobe complexes, have been identified here (Fig. 7). The apex of the Chan Chan trap is displayed on seismic line A-A′ in figure 15.

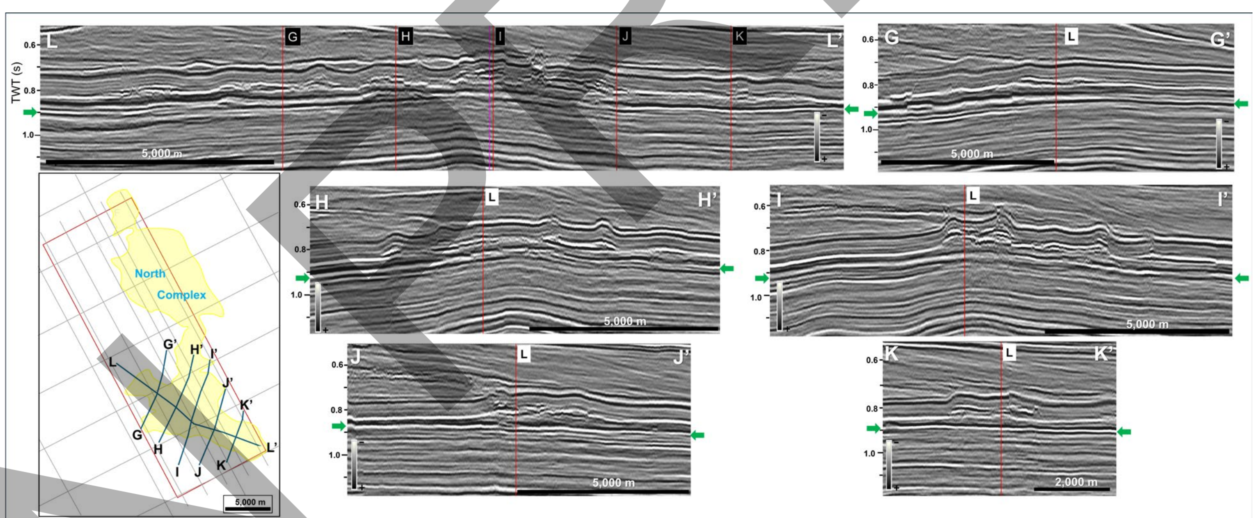

Fig. 16. Chan Chan channel-levee-fan complex. The outline of the 3D survey is shown in red. 2D seismic network shown as gray lines. Yellow area on map shows the extent of the Chan Chan and North channel-levee-fan complexes. Seismic sections G-G’ to K-K’ illustrate the internal architecture of the complex, whereas the L-L’ arbitrary 3D line highlights its lateral extent and geometry. Green arrows on the seismic sections indicate the basal boundary of sequence F, on which the Chan Chan Complex developed. Inferred paleoflow direction is from SE to NW. Differential compaction over channelized, sand-rich deposits enhances the flat-to-convex, domal geometry of the complex, suggesting the presence of a potential stratigraphic trap. The interpreted crest of this trap is marked by a purple vertical line along section L-L’.

The red vertical lines in the profiles indicate the position of the intersecting profiles. Scale bars indicate the polarity of seismic data. TWT: two-way travel time.

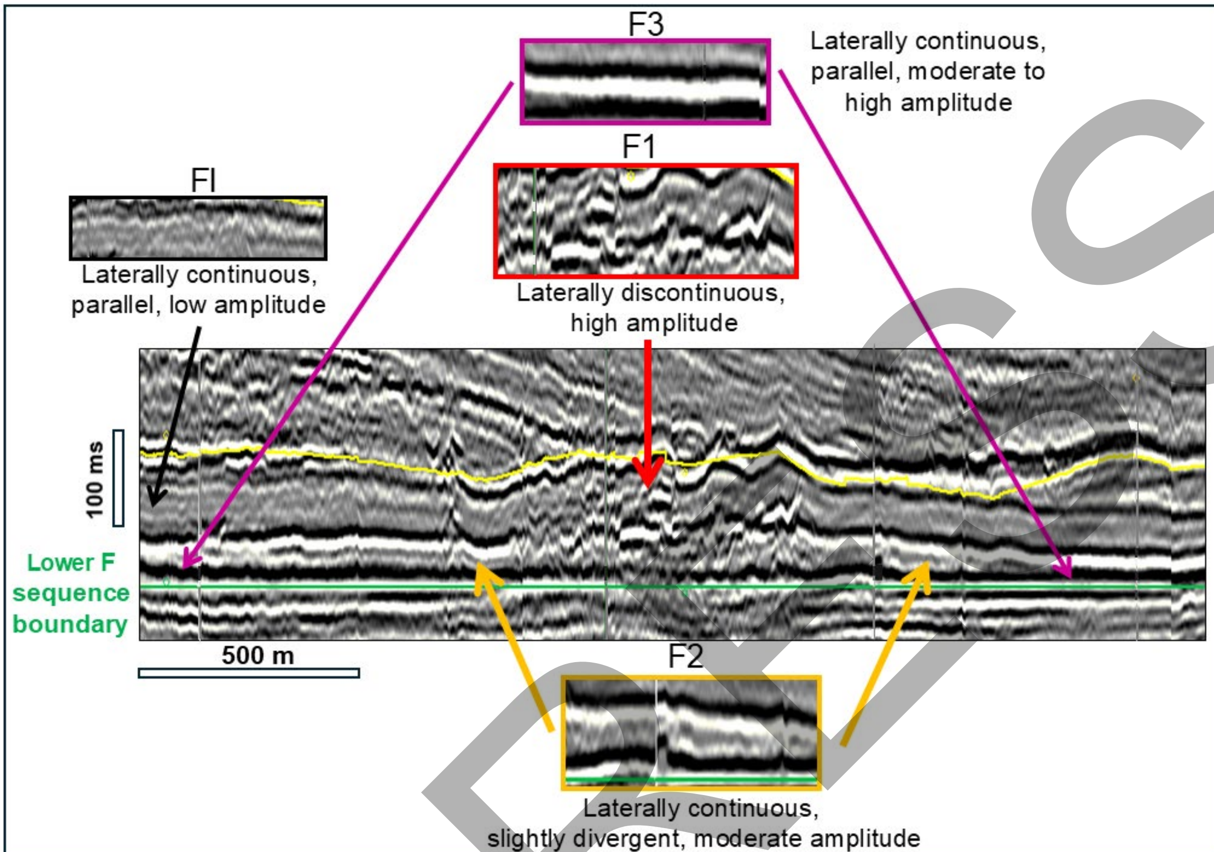

Fig. 17. SW-NE cross section of seismic facies of the Chan Chan Complex, extracted from seismic line L-L' in figure 16 and flattened at the base of sequence F (green horizontal line). The yellow horizon marks the upper boundary of sequence F, which corresponds to the base of the C-MTC megasequence. Note the downlapping clinoforms onto this boundary, indicating progradation at the onset of C-MTC. Seismic facies F1 and F2 correspond to sand-prone channels, with F1 represented by high-amplitude reflection packets (HARPs) and exhibiting a higher sand-to-mud ratio than F2. A progressive decrease in sand content is inferred from F1→F2→F3, with F3 interpreted as distal levee deposits. The overlying FI facies, characterized by low-amplitude to transparent reflections, shows thickness expansion on both flanks of the channel axis, likely due to differential compaction over sand-rich channel fills. See text for discussion.

5. Discussion

5.1. Basin evolution and megasequences

In active subduction-margin settings, high rates of tectonic deformation are typically the dominant control on basin-fill architecture, primarily through their influence on the creation or destruction of accommodation space, whereas sediment supply is generally less well constrained (Paquet et al., 2009). Forearc basins are commonly characterized by spatially and temporally variable patterns of uplift and subsidence associated with local structural activity. In the case of the Salaverry Basin, the uplift and inversion of the adjacent Trujillo Basin influenced its western margin (i.e., the OSH). The distribution of sequence A, along with its correlation with the Ballena 1X and Delfin 1X wells (Figs. 3 and 4), suggests that during much of the Eocene, the OSH did not yet exist as a trench-parallel topographic barrier. Instead, sedimentation occurred within a single, broad forearc basin: the Trujillo Basin. The presence of a thin Eocene section restricted to the seaward margin of the Salaverry Basin, as observed in the Ballena 1X well (Figs. 2 to 4), supports the interpretation of a unified forearc system, dominated by coastal to deep marine depositional environments and fed by trench-orthogonal drainage systems. Most of the Eocene strata lap on the seaward (western) margin of the OSH and expand westward into the Trujillo Basin (Fig. 2).

After an initial transgressive period at the lower part of sequence B, the remainder of the megasequence R (upper part of sequence B through sequence E) represents sedimentation in a deep water (outer neritic to upper bathyal) setting under sand-starved, underfilled conditions. This interpretation is confirmed by micropaleontological content found in the Ballena 1X well (Okada, 1990). Sequences D and E locally display clinoforms prograding from the OSH into the basin with increasing accommodation in shallow waters, without evident erosion on the OSH itself (Fig. 6). This restricted accommodation on the OSH during deposition of sequences D and E, as contrasted with the erosion of underlying sequences, indicates a waning phase of uplift. Conversely, the eastern (landward) margin of the basin is characterized by progressively onlapping contacts (Fig. 8A), reflecting a successive landward encroachment of the basin (Valencia et al., 2013).

Stratal terminations within megasequence S (sequence F) along the western basin margin range from angular truncation to onlap and draping over the OSH, suggesting variable and intermittent uplift of this structure. This megasequence is characterized by transparent seismic facies with high continuity and low-amplitude, parallel to sub-parallel reflectors. Like the underlying sequence E, it thickens over the OSH and records a major flooding event within the basin. Two channel-levee complexes are positioned at the base of this megasequence near the basin center.

The subsequent overfilled stage, corresponding to the "shelved shallow marine variant" of Dickinson (1995), is represented by deltaic clinoforms of the C-MTC megasequence, locally disrupted by slumping. The orientation of clinoform progradation suggests a northward, trench-parallel drainage during this final stage (Azalgara, 1993). This terminal phase of basin evolution reflects landward narrowing and tilting driven by uplift of the OSH, resulting in a marked reduction in accommodation space and/or an increase in sediment supply. A comparable post-tilting, sand-dominated infill stage was described by Buchs et al. (2015) for the present-day evolution of the Kumano forearc basin of south Japan.

5.2. Outer ridge uplift

Extensional, non-accretionary-type forearc basins generally experience minimal compressional deformation and are instead dominated by subsidence (Noda, 2016). The Salaverry Basin, floored by stretched continental crust, is classified as a “residual” forearc basin, with most of its sedimentary fill deposited in a deep-water setting (Allen and Allen, 2013). Active subduction erosion and associated extensional strain, particularly along its western margin, have controlled the development of normal faulting and subsidence within the basin (Clift et al., 2003; Romero et al., 2011, 2013; Witt et al., 2011). Tectonic uplift and inversion of the Trujillo Basin (Prudhomme et al., 2019; Baby et al., 2025) affected its seaward margin, particularly along the OSH (Fig. 18). Comparable deformation patterns and landward tilting of strata at the seaward basin margin have been documented in the adjacent Lima Basin (Krabbenhöft et al., 2004).

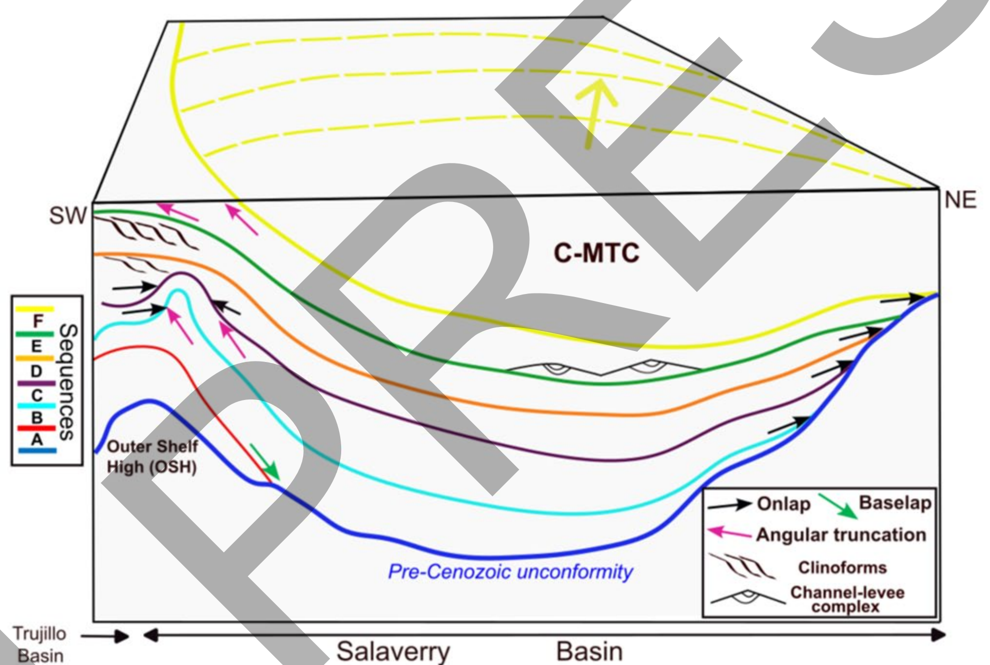

Fig. 18. Summary of key stratal terminations and sequence stratigraphy in the central Salaverry Basin, highlighting two major uplifts affecting its western (seaward) margin: the OSH. The initial phase resulted in the erosion of sequences A and B. Sequence C typically exhibits angular truncation, while sequence D thins and drapes over the OSH, with eastward (basinward) clinoform progradation in its upper section on the eastern OSH flank. Sequence E shows also basinward progradation, as indicated by the presence of clinoforms on the OSH. Sequence F is characterized by substantial thickening over the OSH, with channel levee complexes resting on its lower boundary and entering the basin from the southeast. A subsequent late uplift phase caused tilting and erosion. Northerly clinoform progradation in megasequence C-MTC indicates axial sediment flow in a confined basin. The stratal terminations of sequences B through F along

the eastward (landward) basin margin are characterized by progressive onlaps. Sketch interpreted from figure 4. See text for discussion.

While some interpretations propose a continuous uplift of the OSH from the late Middle Miocene to the Pliocene (Azalgara, 1993), this study instead supports a punctuated uplift model (Fig. 18). Sequences A and B were eroded along the seaward margin of the Salaverry Basin, marking the first phase of uplift. The overlying sequences (C- F), exhibit distinct stratal terminations; for example, sequence C tends to show angular truncation (Fig. 6) or onlap (Fig. 7), while sequence D generally thins and drapes over the OSH with local clinoform progradation (Fig. 6). In contrast, sequences E, in shallow water settings with limited accommodation over the OSH (Fig. 6), and F, in deeper water environments, clearly thicken over the high (Fig. 4), expanding the Miocene section into the adjacent Trujillo Basin (Figs. 2 and 3). This thickening, due to accelerated subsidence beginning late in sequence E and accelerating further during sequence F, along the eastern flank of the OSH, suggests that deposition occurred during a period of relative tectonic quiescence (Fig. 18). The final uplift phase is interpreted as corresponding to the Late Pliocene event identified by Azalgara (1993), which affected not only the OSH and the Trujillo Basin but also extended southeastward to the Lima Basin margin. This uplift episode tilted sequences E and F, whose upper stratal terminations are marked by angular truncation against the modern seafloor (Fig. 6).

The initial phase of uplift resulted in the subdivision of the overlying basin into two distinct depocenters. During this time, sediment supply from the eastern (landward) margin was dominant, as indicated by the deepwater channels in sequences B and C, suggesting a drainage system oriented orthogonally to, or at a high angle with, both the OSH and the trench. The OSH appears to have acted as a significant topographic barrier, locally separating the accretionary prism from the inner forearc depocenters. However, it did serve only intermittently as a major provenance area for the Salaverry Basin. Similar examples can be found elsewhere, Buchs et al. (2015), for instance, described the Kumano forearc basin (Japan), which is separated from the outer depocenter (Nankai Trough) by an outer ridge or trench-slope break (Kimura et al., 2007), as exhibiting limited longitudinal sediment transport within the upper forearc. Instead, the rapid sediment influx driven by mountain building along the landward basin margin has controlled the recent evolution of both the Kumano Basin and the Nankai Trough (Kimura et al., 2018). Likewise, continent-derived sediment supply through punctuated periods of subsidence and uplift/erosion of the trench slope break has been also documented for the Sanriku-Oki forearc basin of northeast Japan by Takano et al. (2025). All these findings support the conclusion that transverse canyons originating on the landward side have played a major role in sediment routing during forearc basin development (Allen and Allen, 2013), and that long-distance longitudinal sediment transport along convergent margins is generally confined to the near-trench environment, even in the presence of extensive forearc basins.

5.3. Sand fairways in an elongate forearc basin

Although sand detection using seismic facies and/or amplitude was not always resolvable with the available seismic data, several sand-rich levels were identified in this study. A transgressive complex is recognized at the base of sequence B, developed over the Chan Chan basement high in the central part of the basin. This unit rests on the pre-Cenozoic unconformity and represents the initial stage of basin infill. The remainder of the succession was deposited under progressively deeper marine conditions, culminating in the basin-wide marine flooding event recorded by sequence F (megasequence S). While some authors interpret the sinuous channels of the megasequence R as part of a fluvial system (Timoteo et al., 2018), evidence from the Ballena 1X well points toward deposition in sand-poor, deep marine environments. Specifically, the Miocene section in Ballena 1X displays a fining-upward trend, and paleobathymetric indicators based on benthic foraminiferal biofacies (Okada, 1990) support outer shelf to upper bathyal settings (Fig. 3). This micropaleontological evidence confirms that much of the Miocene fill was deposited under deep-water, low-energy conditions, consistent with an underfilled, mud-dominated forearc basin. Evidence of wave-base scour in shallow waters is only indicated by the areally restricted clinoforms in sequences D and E, which prograde from the OSH towards the basin center (Figs. 6C and 18). Isolated sands in the uppermost section of sequence E are interpreted as linear shelf sand ridges, encased in fine-grained sediments and oriented parallel to sub-parallel with the basin margin. The orthogonal to highly oblique drainage system from the eastern (landward) margin toward the OSH and trench suggests that, although the OSH acted as a topographic barrier, it did not serve as a significant source of sand identified in the basin center, as exemplified by the eastward-derived sinuous channels in sequence B. Strata along the seaward (western) margin of the basin were deformed and tilted landward as a result of uplift of the OSH. While progressive onlapping contacts are observed along the landward margin throughout the megasequence R, the depocenters associated with each of its sequences appear to have maintained a relatively stable position (Figs. 4 and 18).

Northerly axial sediment supply is inferred in the last phase of the basin fill in megasequences S and C-MTC (Fig. 18). The North and Chan Chan channel-levee complexes (sequence F of megasequence S) and the large clinoforms of megasequence

C-MTC (Fig. 5), show SE to NW flow. This, alongside minor northward clinoforms identified in sequence E (Fig. 5), supports the presence of axial sand transport within the Salaverry Basin.

Concluding remarks

The integrated analysis of regional seismic data and a 3D seismic survey identified three major megasequences (and associated depositional sequences) within the Miocene-Pliocene succession of the central Salaverry Basin, a forearc basin along the Peruvian margin. In ascending stratigraphic order, the megasequences are:

Megasequence R (Sequences A–E): a basin-wide succession characterized by moderate- to high-amplitude, parallel to discontinuous seismic facies, reflecting alternating fine-grained background sedimentation and sand-rich intervals.

Megasequence S (Sequence F): records the basin's maximum transgression and is characterized by transparent to parallel seismic facies indicative of fine-grained sedimentation. Reflectors thicken westward and onlap the eastern basement. Two channel-levee complexes (Northern and Chan Chan) occur along its basal boundary.

Megasequence C-MTC: represents the peak retrogradational phase and is restricted to the basin center. It comprises northward-prograding clinoforms associated with widespread mass transport complexes, reaching ~430 m in thickness and extending ~20 km, indicating strong axial sediment transport.

Seismic stratigraphy records episodic uplift of the Outer Shelf High (OSH). Initial uplift caused erosion of Sequences A and B along the western basin margin. Subsequent sequences document progressive uplift, including erosion of Sequence C, draping and eastward progradation in Sequence D, continued progradation in Sequence E, and westward thickening of Sequence F, indicating increased accommodation over the OSH.

The Salaverry Basin was filled predominantly under underfilled, deep-marine (outer neritic to upper bathyal) conditions, supplied mainly by trench-orthogonal sediment input from the eastern margin. A later reduction in accommodation, driven by renewed OSH uplift and inversion of the adjacent Trujillo Basin, shifted the basin to an oversupplied state characterized by prograding deltaic clinoforms.

ACKNOWLDGMENTS

The author acknowledges SAVIA Peru S.A. for supplying the seismic and well data used in this contribution. Beneficial discussions with J. Fuentes, K. Andamayo, K. Valencia and E. Borda are thanked. The journal reviewers, P. Baby and T. McHargue, are gratefully acknowledged for their constructive reviews. The journal editor, D. Bertin, is also acknowledged for his time and effort in providing valuable feedback on the manuscript.

REFERENCES

Aitken, T.; Mann P., Escalona A., Christeson G. 2011. Evolution of the Grenada and Tobago basins and implications for arc migration. Marine and Petroleum Geology 28: 235–258. https://doi:10.1016/j.marpetgeo.2009.10.003

Allen, P.A.; Allen, J.R. 2013. Basin Analysis: Principles and Application to Petroleum Play Assessment, Blackwell Publishing, third edition, 640 p.

Azalgara, C. 1993. Structural evolution of the offshore forearc basins of Peru, including the Salaverry, Trujillo, Lima, West Pisco and East Pisco Basins. Master Thesis (Unpublished), Rice University, Houston, Texas, 168 p.

Babonneau, N.; Savoye, B., Cremer, M., Klein, B. 2002. Morphology and architecture of the present canyon and channel system of the Zaire deep-sea fan. Marine and Petroleum Geology 19 (4): 445–467. https://doi.org/10.1016/S0264-8172(02)00009-0

Baby, P.; Prudhomme, A., Brusset, S., Robert, A., Roddaza, M., Calderon, Y., Eudec, A., Willy, G., Hermoza, W., Hurtado, C., Brichau, S., Calvès, G., Pierre-Olivier Antoine, P-A, Salas-Gismondi, R. 2025 The Northern Central Andes and Andean tectonic evolution revisited: An integrated stratigraphic and structural model of three superimposed orogens, Earth-Science Reviews 260: 104998. https://doi.org/10.1016/j.earscirev.2024.104998

Bacon, M.; Simm R., Redshaw, T. 2003. 3-D Seismic Interpretation, Cambridge University Press: 207p.Cambridge. https://doi.org/10.1017/CBO9780511802416

Bassetti, M. A.; Jouet, G., Dufois, F., Berné, S., Rabineau, M., Taviani, M. 2006. Sand bodies at the shelf edge in the Gulf of Lions (Western Mediterranean): Deglacial history and modern processes. Marine Geology 234(1-4): 93–109. https://doi.org/10.1016/J.MARGEO.2006.09.010

Baudon, C.; Cartwright, J. 2008. Early stage evolution of growth faults: 3D seismic insights from the Levant Basin, Eastern Mediterranean. Journal of Structural Geology 30(7): 888–898. https://doi.org/10.1016/j.jsg.2008.02.019

Beaudry D.; Moore, G. 1985. Seismic Stratigraphy and Cenozoic Evolution of West Sumatra Forearc Basin. American Association of Petroleum Geologists Bulletin 69(5): 742-759. https://doi.org/10.1306/AD4627FE-16F7-11D7-8645000102C1865D

Benavides, V. 1999, Orogenic evolution of the Peruvian Andes: The Andean cycle. *In* Geology and Mineral Deposits of Central Andes (Skinner, B.; editor). Society of Economic Geology, Special Publication 7: 61–108. Tulsa. https://doi.org/10.5382/SP.07.03

Bourgois J.; Huchon P., Pautot G. 1990, Geología de la margen activa del Perú entre los 3° y 12° de latitud Sur. Bulletin de l'Institut Français d'Études Andines, 19(2) : 241-291. https://doi.org/10.3406/bifea.1990.1007

Brewster, J. 1991. The Frigg Field, Block 10/1 UK North Sea and 25/1, Norwegian North Sea. *In*: United Kingdom Oil and Gas Fields, 25 Years Commemorative Volume (Abbotts, I.L.; editor) Geological Society, London, Memoir 14: 117-126. https://doi.org/10.1144/GSL.MEM.1991.014.01.15

Buchs, D. M.; Cukur D., Masagoc H., Garbe-Schönberg, D. 2015. Sediment flow routing during formation of forearc basins: Constraints from integrated analysis of detrital pyroxenes and stratigraphy in the Kumano Basin, Japan, Earth and Planetary Science Letters 414:164-175. http://dx.doi.org/10.1016/j.epsl.2014.12.046

Butler, R.W. 2019 Syn-kinematic strata influence the structural evolution of emergent fold–thrust belts. *In*: Fold and Thrust Belts: Structural Style, Evolution and Exploration (Hammerstein, J.A., Di Cuia, R., Cottam, M. A., Zamora, G., Butler R.W.; editors). Geological Society, London, Special Publications, 490. https://doi.org/10.1144/SP490-2019-14

Calvès, G.; Auguy, C., de Lavaissière, L., Brusset, S., Calderon, Y., Baby, P. 2017. Fore-arc seafloor unconformities and geology: insight from 3-D seismic geomorphology analysis, Peru. Geochemistry,Geophysics, Geosystems 18: 3062-3077. https://doi.org/10.1002/2017GC007036

Canchanya, Z.; Paz, M. 1992, Estudio Bioestratigráfico en base a nannoplancton calcáreo: Pozo Delfin–1X y Ballena–1X, Cuenca Salaverry: Petroperú, unidad de investigación y desarrollo, Unpubished report, pp. 14.

Cattaneo, A.; Steel, R. 2003. Transgressive deposits: a review of their variability. Earth Science Review (62):187-228. https://doi.org/10.1016/S0012-8252(02)00134-4

Catterall, V.; Redefern J., Gawthorpe R., Hansen D., Thomas, M. 2010. Architectural style and quatification of a submarine channel-levee system located in a structurally complex area: offshore Nile Delta. Journal of Sedimentary Research 80: 991-1017. https://doi.org/10.2110/jsr.2010.084

Chiarella, D.; Longhitano, S., Mosdell W., Telesca, D. 2020. Sedimentology and facies analysis of ancient sand ridges: Jurassic Rogn Formation, Trøndelag Platform, offshore Norway, Marine and Petroleum Geology 112, 104082. https://doi.org/10.1016/j.marpetgeo.2019.104082

Childs, C., A. Nicol, J. Walsh, J. Watterson, 2003. The growth and propagation of synsedimentary faults Journal of Structural Geology 25(4): 633-648. https://doi.org/10.1016/S0191-8141(02)00054-8

Chopra, S.; Marfurt, K.J. 2012. Seismic Attribute Expression of Differential Compaction, Leading Edge 31(12): 1418–1422. https://doi.org/10.1190/segam2012-1323.1

Clift, P. D.; Pecher, I., Kukowski, N, Hampel, A. 2003. Tectonic erosion of the Peruvian forearc, Lima Basin, by subduction and Nazca Ridge collision: Tectonics 22(3), 1023. https://doi.org/10.1029/2002TC001386

Clifton, H.E. 2006. A re-examination of facies models for clastic shorelines. *In* Facies Models Revisited (H. W. Posamentier, H.W.; Walker, R.G.; editors) SEPM Society for Sedimentary Geology Special Publication 84: 293-337. https://doi.org/10.2110/pec.06.84.0293

Coleman, A.; Duffy O., Jackson C. 2019. Growth folds above propagating normal faults. Earth-Science Reviews, v.196,102885. https://doi.org/10.1016/j.earscirev.2019.102885.

CoreLab 2012. Peru Reservoirs and Seals - Offshore Basins. Report (Unpublished): 74 p.

Cross, N.E.; Cunningham, A., Cook, R.J., Taha, A., Esmaie, E., El Swidan, N. 2009. Three-dimensional seismic geomorphology of a deep-water slope-channel system: the Sequoia field, offshore west Nile Delta, Egypt. American Association of Petroleum Geologists Bulletin 93: 1063-1086. https://doi.org/10.1306/05040908101

Cuipa Vicencio, J.P. 2018. Análisis estructural y sistema petrolero de las cuencas de Antearco, Trujillo Sur y Salaverry norte, centro de Perú, Tesis de pregrado (Unpublished), Universidad Nacional Mayor de San Marcos: 193 p. Lima.

Curray, J.R. 1964. Transgressions and regressions. *In*: Papers in Marine Geology (Miller, R.L.; editor) Macmillan: 175-203. New York.

Daudt, J.; Scherer, C.M. 2006. Arquitetura de fácies e evolução estratigráfica dos reservatórios flúvio-deltaicos da Formação Echinocyamus (Eoceno Inferior) na área do Lote 10 (Bacia de Talara, Noroeste do Peru). Boletim de Geociências da Petrobras 14: 27-45.

Demarest J. M.; Kraft J. C., 1987. Stratigraphic record of Quaternary sea levels: implication for more ancient strata. *In* Sea-level fluctuation and coastal evolution. (Nummedal, D.O.; Pilkey, H.; Howard J.D.; editors). SEPM Society for Sedimentary Geology Special Publication 41: 223 – 239. Tulsa. https://doi.org/10.2110/pec.87.41.0223

Deptuck, M.E.; Sylvester, Z., Pirmez, C., O'Byrne, C. 2007. Migration-aggradation history and 3-D seismic geomorphology of submarine channels in the Pleistocene Benin-major Canyon, western Niger Delta slope. Marine and Petroleum Geology 24: 406–433. https://doi.org/10.1016/j.marpetgeo.2007.01.005

Díaz, F.; Salguero, E., Matava,T., 2019. New Insights on the Petroleum System in the Salaverry Basin-Offshore Peru, First HGS and EAGE Conference on Latin America: 1 p. Houston. https://doi.org/10.3997/2214-4609.202180004

Dickinson, W.R. 1973. Widths of modern arc-trench gaps proportional to past duration of igneous activity in associated magmatic arcs. Journal of Geophysical Research 78 (17): 3376–3389. https://doi.org/10.1029/JB078i017p03376

Dickinson, W.R. 1974. Plate Tectonics and Sedimentation: Society of Economic Paleontologists and Mineralogists, Special Publication 22: 1–27. Tulsa. https://doi.org/10.2110/pec.74.22.0001

Dickinson, W.R. 1995, Forearc Basins. *In*: Tectonics of Sedimentary Basins (Busby, C.J.; R. V. Ingersoll; editors) Blackwell Science: 221–262.

Dickinson, W. R.; Seely, D. R. 1979. Structure and stratigraphy of forearc regions. American Association of Petroleum Geologists Bulletin 63(1): 2–31. https://doi.org/10.1306/C1EA55AD-16C9-11D7-8645000102C1865D

Draut, A.; Clift, P. 2012. Basins in arc-continent collisions. *In* Tectonics of Sedimentary Basins: Recent Advances (Busby, C.A.; Azor, A., editors). Blackwell Publishing Ltd.: 347-368. https://doi.org/10.1002/9781444347166

Dunbar, R.B.; Marty R.C., Baker, P.A., 1990. Cenozoic marine sedimentation in the Sechura and Pisco Basins, Peru. Palaeogeography Palaeoclimatology Palaeoecology 41: 235–261. https://doi.org/10.1016/0031-0182(90)90179-B

Emery, D.; Myers, K.J. 1996. Sequence Stratigraphy. Blackwell Publishing Ltd: 297 p. Oxford. DOI:10.1002/9781444313710

Eschard, R. ; Albouy, E., Deschamps, R., Euzen, T., Ayu, A. 2013. Downstream evolution of turbiditic channel complexes in the Pab Range outcrops (Maastrichtian, Pakistan). Marine and Petroleum Geology 20: 691–710. https://doi.org/10.1016/j.marpetgeo.2003.02.004

Fildani A.; Hanson D.H., Zhengzheng C., Moldowan J.M., Graham S.A., Arriola P.R. 2005. Geochemical characteristics of oil and source rocks and implications for petroleum system, Talara

Basin, northwest Peru. American Association of Petroleum Geologists Bulletin 89(11): 1519-1545. https://doi.org/10.1306/06300504094

Fildani, A.; Hessler, A.M., Graham, S.A. 2008. Trench forearc interactions reflected in the sedimentary fill of Talara basin, northwest Peru. Basin Research 20: 305–331. https://doi.org/10.1111/j.1365-2117.2007.00346.x

Flood, R. D.; Manley, P. L., Kowsmann, R. O., Appi, C. J., Pirmez, C. 1991. Seismic Facies and Late Quaternary Growth of Amazon Submarine Fan. *In* Seismic Facies and Sedimentary Processes of Submarine Fans and Turbidite Systems. Frontiers in Sedimentary Geology (P. Weimer, P; Link, M.H.; editors). Springer-Verlag: 415-433. New York. https://doi.org/10.1007/978-1-4684-8276-8_23

Fonnesu, F. 2003. 3D seismic images of a low-sinuosity slope channel and related depositional lobe (West Africa deep-offshore), Marine and Petroleum Geology 20: 615–629. https://doi.org/10.1016/j.marpetgeo.2003.03.006

Gawthorpe, R.L.; Sharp, I., Underhill, J.R., Gupta, S. 1997. Linked sequence stratigraphic and structural evolution of propagating normal faults. Geology 25 (9): 795-798. https://doi.org/10.1130/0091-7613(1997)025<0795:LSSASE>2.3.CO;2

Genge, M. C.; Witt, C., Chanier, F., Reynaud, J.Y., Calderon, Y. 2020. Outer forearc high control in an erosional subduction regime: The case of the central Peruvian forearc (6–10°S). Tectonophysics, 228546. 10.1016/j.tecto.2020.228546

Gervais, A.; B. Savoye, D. Piper, T. Mulder, M. Cremer, L. Pichevin 2004. Present morphology and depositional architecture of a sandy confined submarine system: the Golo turbidite system (eastern margin of Corsica). *In*: Confined Turbidite Systems (Lomas, S.; Joseph P.; editors.) Geological Society, London, Special Publication 222: 59-89. https://doi.org/10.1144/GSL.SP.2004.222.01.05

Giles, K. A. 2010. Tracking the Migration of Salt Diapirs Using Halokinetic Sequence Stratigraphy. American Association of Petroleum Geologists Search and Discovery Article #40534.

Giles, K.A.; Lawton, T.F. 2002, Halokinetic sequence stratigraphy adjacent to the El Papalote diapir, northeastern Mexico. American Association of Petroleum Geologists Bulletin 86: 823-840. https://doi.org/10.1306/61EEDBAC-173E-11D7-8645000102C1865D

Giles, K.A.; Rowan, M.G. 2012. Concepts in halokinetic-sequence deformation and stratigraphy. *In* Salt Tectonics, Sediments and Prospectivity (Alsop, G.I.; Archer, S.G.; Hartley, A.J.; Grant, N.T.; Hodgkinson, R.; editors) Geological Society, London, Special Publication 363: 7-32. https://doi.org/10.1144/SP363.2

Gong, C.; Steel R., Olariu, C., Xu, Q., Liu, X., Zhao Q. 2015. Growth Styles of Shelf-Margin Clinoforms: prediction of sand- and sediment-budget partitioning into and across the shelf. Journal of Sedimentary Research 85: 209–229. https://doi.org/10.2110/jsr.2015.10

Gonzales, E. 2014. Biostratigraphy chart Salaverry Basin Chan Chan area: Based on microfossils (planktonic, benthonic, nanno, pollen and spores): SAVIA Peru S.A. Internal Report, p. 38.

Haq, E.; Youliang, J., Ulla, H., Shahzad K., Ahmed, Mashwani, N., Zaheer, M. 2023. Architectural complexities and morphological variations of the Indus fan and its elements: Understanding of the turbidite system through seismic characterization. Marine and Petroleum Geology 150: 106103. https://doi.org/10.1016/j.marpetgeo.2023.106103

Hampel, A. 2002. The migration history of the Nazca Ridge along the Peruvian active margin: A re-evaluation. Earth Planetary Science Letters, 203: 665–679. https://doi.org/10.1016/S0012-821X(02)00859-2

Hay-Roe, H.; Miller, P. 1992. Portachuelo Field--Peru Talara Basin, in: Structural Traps VII, American Association of Petroleum Geologists Treatise: 245-266. Tulsa.

Helland-Hansen, W.; Gjelberg, H. 2012 Towards a Hierarchical Classification of Clinoforms. American Association of Petroleum Geologists Search and Discovery Article #90142, AAPG Annual Convention and Exhibition, Long Beach.

Heritier, E. E.; Lossel, P., Wathne, E. 1979. Frigg Field-large submarine fan trap in lower Eocene rocks of North Sea Viking Graben. American Association of Petroleum Geologists Bulletin 63(11): 1999-2020. https://doi.org/10.1306/2F918856-16CE-11D7-8645000102C1865D

Higley, D. 2004. The Talara Basin Province of Northwestern Peru: Cretaceous-Tertiary Total Petroleum System, U.S. Geological Survey Bulletin 2206-A, 28 p. https://doi.org/10.3133/b2206A

Horton, B.; Yin A., Spurlin, M. S., Zhou J., Wang, J. 2002. Paleocene–Eocene syncontractional sedimentation in narrow, lacustrine-dominated basins of east-central Tibet. Geological Society of America Bulletin 114 (7): 771–786. https://doi.org/10.1130/0016-7606(2002)114<0771:PESSIN>2.0.CO;2

Hubbard, R.J. 1988. Age and significance of sequence boundaries on Jurassic and Early Cretaceous rifted continental margins, American Association of Petroleum Geologists Bulletin 72: 49-72. https://doi.org/10.1306/703C81C8-1707-11D7-8645000102C1865D

Hubbard, R.J.; Pape, J., Roberts, D.G. 1985. Depositional sequence mapping as a technique to establish tectonic and stratigraphic framework and evaluate hydrocarbon potential on a passive margin. In: Seismic Stratigraphy 11 (Berg, O.R., Woolverton, D.; editors),, American Association of Petroleum Geologists, 39: 79–91. Tulsa. https://doi.org/10.1306/M39449C5

Hubbard, S.M.; de Ruig, M. Graham, S. 2009. Confined channel-levee complex development in an elongate depo-center: Deep-water Tertiary strata of the Austrian Molasse basin, Marine and Petroleum Geology 26: 85–112. https://doi.org/10.1016/j.marpetgeo.2007.11.006

Ibaraki, M. 1990. Eocene through Pleistocene planktonic foraminifers off Peru, leg 112; biostratigraphy and paleoceanography. Presented at the Proceedings of the Ocean Drilling Program Scientific Results 112: 239-262.

Ingersoll, R.V. 1988. Tectonics of sedimentary basins, Geological Society of America Bulletin, 100: 1704-1719. https://doi.org/10.1130/0016-7606(1988)100<1704:TOSB>2.3.CO;2

Jobe, Z. R.; Howes N., Auchter, N., 2016. Comparing submarine and fluvial channel kinematics: Implications for stratigraphic architecture, Geology 44(11): 931-934. https://doi.org/10.1130/G38158.1

Jolly, B.A.; Lonergan, L., Whittaker, A.C. 2016. Growth history of fault-related folds and interaction with seabed channels in the toe-thrust region of the deep-water Niger Delta. Marine and Petroleum Geology, 70, 58e76. https://doi.org/10.1016/j.marpetgeo.2015.11.003

Karig, D.E. 1974. Evolution of arc systems in the western Pacific. Annual Review of Earth and Planetary Sciences 2 (1): 51–75. https://doi.org/10.1146/annurev.ea.02.050174.000411

Karig, D.E.; Sharman, G.F. 1975. Subduction and accretion in trenches: Geological Society of America Bulletin 86 (3): 377–389. https://doi.org/10.1130/0016-7606(1975)86<377:SAAIT>2.0.CO;2

Kimura G.; Kitamura, Y., Hashimoto Y., Yamaguchi, A., Shibata T., Ujiie K., Okamoto, S. 2007. Transition of accretionary wedge structures around the up-dip limit of the seismogenic subduction zone. Earth Planetary Science Letters 255: 471–484. https://doi.org/10.1016/j.epsl.2007.01.005

Kimura, G.; Koge H., Takeshi, T., 2018. Punctuated growth of an accretionary prism and the onset of a seismogenic megathrust in the Nankai Trough, Progress in Earth and Planetary Science, 5:78. https://doi.org/10.1186/s40645-018-0234-1

Kjøll, J.J.; Midtkandal, I., Manton, B., Planke, S. 2025. Seismic Geomorphology of an Early Eocene Canyon- Channel- Lobe System North of Shetland, Basin Research, 2025; 37:e70031. https://doi.org/10.1111/bre.70031

Krabbenhöft, A.; Bialas, J., Kopp, H., Kukowski, N., Hübscher, C. 2004. Crustal structure of the Peruvian continental margin from wide-angle seismic studies: Geophysical Journal International 159(2), 749-764. https://doi.org/10.1111/j.1365-246X.2004.02425.x

Kukowski, N.; Oncken, O. 2006. Subduction Erosion — the "Normal" Mode of Fore-Arc Material Transfer along the Chilean Margin? *In* The Andes. (Oncken, O; Chong, G.; Franz, G.; Giese, P.; Götze, H.; Ramos, V.A.; Strecker, M.; Wigge, P.; editors). Frontiers in Earth Sciences. Springer, Chapter 10: 217-236. Heidelberg. https://doi.org/10.1007/978-3-540-48684-8_10

Kulm L. D.; Schweller W.J., Masias A., 1977. A preliminary analysis of the subduction process along the Andean continental margin near 6° to 45°S. *In* Island arcs, deep-sea trenches, and back-arc Basins, (Talwani, M.; W. Pitman, W; editors). AGU Maurice Ewing Series 1: 285–301. https://doi.org/10.1029/ME001p0285Digital Object Identifier (DOI)

Kulm, L. D., Prince R.A., French W., Johnson, S., Masias, A.1981 Crustal structure and tectonics of the central Perú continental margin and trench. Geological Society of America Memoir 154: 445–508. https://doi.org/10.1130/MEM154-p351

Kulm, L.D., Thornburg T.M., Schrader H.J., Resig, J.M. 1982. Cenozoic structure, stratigraphy and tectonics of the central Peru forearc. Geological Society, London, Special Publications, 10(1): 151-169. https://doi.org/10.1144/GSL.SP.1982.010.01.10

Lee, H. J.; Jeon, C. K., Lim, H. S., 2020. Transgressive Shelf Sands around the Korean Peninsula: A Brief Review. Ocean Science Journal 55(4):465–475. https://doi.org/10.1007/s12601-020-0035-5

Lewis, M.; Jackson C. A.-L, Gawthorpe R., Whipp, P. 2015. Early synrift reservoir development on the flanks of extensional forced folds: A seismic-scale outcrop analog from the Hadahid fault system, Suez rift, Egypt. American Association of Petroleum Geologists Bulletin 99 (6): 985-1012. https://doi.org/10.1306/12011414036

Llerena, C.; Valencia, K., Romero, D. Peña, D. 2013. Potenciales reservorios naturalmente fracturados en la cuenca Salaverry relacionados con el magmatismo Hauteriviano-Barremiano (Formación Pucusana): Nuevas dataciones U-Pb y Ar-Ar. Boletín de la Sociedad Geológica del Perú 108: 153-160.

Llerena, C. 2014. Evaluación de los potenciales reservorios naturalmente fracturados en la cuenca Salaverry, a partir del análisis estructural de la costa del Perú central. Tesis de grado (Unpublished). Universidad Nacional de San Agustín: 270 p.

Lopez-Gamundi, O. 2014. Sequence Stratigraphic Evaluation of the Salaverry Basin (Chan Chan 3D) in Block Z-35, with emphasis on reservoir facies. SAVIA Internal Report (unpublished): 80 p.

Macharé J., Sébrier M., Huaman D., Mercier J. 1986. Tectónica cenozoica de la margen continental peruana. Boletín Sociedad Geológica de Perú 76: 45-78.

Maloney, D.; Davies, R., Imber J., Higgins S., Kin S., 2010. New insights into deformation mechanisms in the gravitationally driven Niger Delta deep-water fold and thrust belt. American Association of Petroleum Geologists Bulletin 94 (9): 1401-1424. http://dx.doi.org/10.1306/01051009080

Martínez, E.; Fernandez J., Calderón Y., Hermoza W., Galdos C. 2005. Tumbes and Talara Basins hydrocarbon evaluation: PeruPetro, Exploration Department, Basin Evaluation Group, Internal report (Unpublished): 130 p.

Marty, R.C. 1989. Stratigraphy and chemical sedimentology of Cenozoic biogenic sediments from the Pisco and Sechura Basins, Peru. Ph.D. Thesis, Rice University: 268 p.

McGovney, I.E.; Radovich, B. 1985. Seismic stratigraphy and facies of the Frigg Fan complex, North Sea. *In* Seismic stratigraphy II (Berg, O.R.; Woolverton, D.G.; editors). American Association of Petroleum Geologists Memoir 39: 139-156. https://doi.org/10.1306/M39449C8

McHargue T.; Pyrcz, M. J., Sullivan, M. D., Clark, J. D., Fildani, A., Romans, B. W., Covault, Levy, J., Posamentier H., Drinkwater, N. 2011. Architecture of Turbidite Channel Systems on the continental Slope: Patterns and Predictions. Marine and Petroleum Geology 28: 728–743. https://doi.org/10.1016/j.marpetgeo.2010.07.008

McHargue, T.; Hodgson D.M., Shelef, E. 2021. Architectural diversity of submarine unconfined lobate deposits. Frontiers in Earth Science 9: 697-170. https://doi.org/10.3389/feart.2021.697170

Mégard, F. 1987. Structure and Evolution of the Peruvian Andes. *In* The Anatomy of Mountain Ranges (Schaer, J.P; Rodgers, J.; editors). Princeton University Press:179–210. Princeton.

Menant, A.; Angiboust, S., Gerya, T., Lacassin, R., Simoes, M., Grandin, R. 2020. Transient stripping of subducting slabs controls periodic forearc uplift. Nature Communications 11, 1823. https://doi.org/10.1038/s41467-020-15580-7

Meza, O.; Peralta.V., Nuñez, E. 2010. Influence of Stress Field in the Productivity of Naturally Fractured Reservoirs in Metamorphic Basement: A Case Study of the San Pedro Field, Amotape Group. SPE Latin American and Caribbean Petroleum Engineering Conference. Paper Number: SPE-138946-MS. https://doi.org/10.2118/138946-MS

Minguito, M. A.; Machín, J. Cakebread, J., Beroiz, C.1997. Hydrocarbon potential review, Z-29 block, Trujillo Basin, Perú, Volume I: Geology: Repsol Exploración S.A., Internal Report (Unpublished):105 p.

Mitchum, R.M. 1985. Seismic stratigraphic recognition of submarine fans. *In* Seismic stratigraphy II (Berg, O.R.; Woolverton, D.G.; editors). American Association of Petroleum Geologists Memoir 39: 117-136. https://doi.org/10.1306/M39449C7

Mitchum, R.M.; Vail, P.R. 1977.Seismic stratigraphy and global changes of sea-level, part 6: stratigraphic interpretation of seismic reflection patterns in depositional sequences. *In* Seismic Stratigraphy — Applications to Hydrocarbon Exploration (Payton, C.E.; editor) American Association of Petroleum Geologists Memoir 26: 135–144. https://doi.org/10.1306/M26490C8

Morales, C.; Gonzales, E. 2006. Determinación litológica y bioestratigráfica de los pozos Ballena–1X, Delfin–1X, Lobos–1X y Morsa–1X, Cuenca Trujillo. Petro-Tech Peruana Internal Report (Unpublished) 2 p.

Morley, C.K. 2009. Growth of folds in a deep-water setting. Geosphere 5: 59–89. https://doi.org/10.1130/GES00186.1.

Moxon, I.W.; Graham, S.A., 1987. History and controls of subsidence in the Late Cretaceous Tertiary Great Valley forearc basin, California. Geology 15: 626–629. https://doi.org/10.1130/0091-7613(1987)15<626:HACOSI>2.0.CO;2

Narvaez, J.; Pardo, A. 1993. Nueva fauna fósil del Eoceno del pozo Delfin–1X (Margen continental, norte del Perú): Alcances estratigráficos y tectónicos: Petroperú, Report (Unpublished): 13 p.

Neal, J.; Abreu, V. 2009. Sequence stratigraphy hierarchy and the accommodation succession method. Geology 37: 779-782. https://doi.org/10.1130/G25722A.1

Noda, A. 2016. Forearc basins: Types, geometries, and relationships to subduction zone dynamics. Geological Society of America Bulletin 128 (5-6): 879–895. https://doi.org/10.1130/B31345.1

Noda, A.; Miyakawa, A. 2017. Deposition and Deformation of Modern Accretionary-Type Forearc Basins: Linking Basin Formation and Accretionary Wedge Growth. *In* Evolutionary Models of Convergent Margins - Origin of Their Diversity (Itoh, Y.; editor.). InTech, Chapter 1: 2-27. http://dx.doi.org/10.5772/67559

Nummedal D; Swift D.P 1987. Transgressive stratigraphy at sequence-bounding unconformities: Some principles derived from Holocene and Cretaceous examples. *In* Sea-level fluctuation and coastal evolution (Nummedal, D.; Pilkey, O.H.J.D. Howard, J.D; editors). Society of Economic Paleontologists and Mineralogists Special Publication 41: 241–260. https://doi.org/10.2110/pec.87.41.0241

Okada, H. 1990. Nannofossils biostratigraphy of the Ballena–1X and Delfin–1X wells. *In* Structural Evolution of the Offshore Forearc Basins of Peru, Including the Salaverry, Trujillo, Lima, West Pisco and East Pisco Basins, C. Azalgara (Master Science Thesis). Rice University: 168 p. Appendix A.

Oyedele, O. A.; Dupré W.R., Marfurt, K.J. 2015. Seismic facies analysis and age dating of mid-Pleistocene channel lobe deposits, Mad Dog Field, Gulf of Mexico. AAPG Datapages/Search and Discovery Article #90219. Houston.

Paquet, F.; Proust, J.-N., Barnes, P. M., Pettinga, J. R. 2009. Inner-Forearc Sequence Architecture in Response to Climatic and Tectonic Forcing Since 150 ka: Hawke's Bay, New Zealand. Journal of Sedimentary Research 79(3): 97-124. https://doi.org/10.2110/jsr.2009.019

Paquet, F.; Proust, J.N., Barnes, P. M., Pettinga, J. R. 2011. Controls on active forearc basin stratigraphy and sediment fluxes: The Pleistocene of Hawke Bay, New Zealand. Geological Society of America Bulletin 123(5-6): 1074-1096. https://doi.org/10.1130/B30243.1

PARSEP 2001a. The Salaverry Basin, A study on the Hydrocarbon Potential of the Salaverry. Internal Report (Unpublished): 67 p.

PARSEP 2001b. The Trujillo Basin: a study on the remaining undiscovered hydrocarbon potential of the Trujillo offshore basin, Peru. Internal Report (Unpublished): 109 p.

PeruPetro 1981a. Informe micropaleontológico del pozo Ballena 8-1. Informe técnico IPP21707 (Unpublished): 15 p.

PeruPetro 1981b. Informe micropaleontológico del pozo Delfin 20-X-1 8-1. Informe técnico IPP21709 (Unpublished): 62 p.

PeruPetro 2005. Tumbes and Talara Basins Hydrocarbon Evaluation, Internal Report (Unpublished): 149 p.

Pilger, R.H. 1984. Cenozoic plate kinematics, subduction and magmatism: south American Andes. Journal Geological Society of London 141: 793-802. https://doi.org/10.1144/gsjgs.141.5.0793

Posamentier, H.W. 2002. Ancient shelf ridges - a potentially significant component of the transgressive systems tract: case study from offshore northwest Java. American Association of Petroleum Geologists Bulletin: 86, 75–106. https://doi.org/10.1306/61EEDA44-173E-11D7-8645000102C1865D

Posamentier, H.W. 2003. Depositional elements associated with a basin floor channel levee system: case study from the Gulf of Mexico. Marine and Petroleum Geology 20: 677- 690. https://doi.org/10.1016/j.marpetgeo.2003.01.002

Posamentier, H.W.; Erskine, R.D., 1991. Chapter 10. Seismic Expression and Recognition Criteria of Ancient Submarine Fans. *In* Seismic Facies and Sedimentary Processes of Submarine Fans and Turbidite Systems (Weimer, P; M. H. Link, M.H.; editors). Frontiers in Sedimentary Geology. Springer-Verlag: 197- 222. New York. https://doi.org/10.1007/978-1-4684-8276-8_10

Posamentier, H. W.; Kolla, V. 2003. Seismic Geomorphology and stratigraphy of depositional elements in Deep-Water Settings. Journal of Sedimentary Research 73(3): 367- 388. https://doi.org/10.1306/111302730367

Paton, D.; van der Spuy, D., di Primio, R., Horsfield, B., 2008. Tectonically induced adjustment of passive-margin accommodation space; influence on the hydrocarbon potential of the Orange

Basin, South Africa, American Association of Petroleum Geologists Bulletin 92(5): 589–609. https://doi.org/10.1306/12280707023

Patruno, S.; Helland-Hansen, W., 2018. Clinoforms and clinoform systems: review and dynamic classification scheme for shorelines, subaqueous deltas, shelf edges and continental margins. Earth Science Review 185: 202–233. https://doi.org/10.1016/j. earscirev.2018.05.016.

Prudhomme, A.; Baby, P., Robert, A., Brichau, S., Cuipa, E., Eude, A., Calderon, Y, O'Sullivan, P. 2019. Western thrusting and uplift in northern Central Andes (western Peruvian margin). *In* Andean Tectonics (Horton, B.K.; A. Folguera, A.; editors). Elsevier, chapter 11: 299–331. Amsterdam. 10.1016/B978-0-12-816009-1.00013

Qi, K.; Ding, L., Gong C., H. Wang, D. Shao, Z. Cai, H. Ma, X. Xu, Z. Jin 2021. Different avulsion events throughout the evolution of submarine channel-levee systems: A 3D seismic case study from the northeastern Bengal Fan. Marine and Petroleum Geology 134, 105310. https://doi.org/10.1016/j.marpetgeo.2021.105310

Ramos, V.A. 2009. Anatomy and global context of the Andes: Main geologic features and the Andean orogenic cycle. *In* Backbone of the Americas: Shallow Subduction, Plateau Uplift, and Ridge and Terrane Collision (Kay, S.M; Ramos V.A.; Dickinson, W. R.; editors). Geological Society of America Memoir 204: 31–65. https://doi.org/10.1130/2009.1204(02)

Roeder, D. 2012. Convergent margins and orogenic belts. *In* Regional Geology and Tectonics: Principles of Geologic Analysis (Roberts, D. G.; Bally, A.W.; editors), Regional Geology and Tectonics: Principles of Geologic Analysis, Elsevier: 112–177. Amsterdam. 10.1016/B978-0-444-53042-4.00006-6

Reinson, G.E. 1992. Transgressive barrier island and estuarine systems. *In* Facies Models - Response to Sea Level Change (Walker, R.G.; James, N.P.; editors). Geological Association of Canada Publications, Geotext 1: 179–194.

Romero, D.; Venturo, D., Valencia, K. 2010. Evolución Tectono-sedimentaria del margen continental durante el Jurásico-Cretácico, costa afuera del Perú Central. XV Congreso Peruano de Geología, Resúmenes Extendidos, Sociedad Geológica del Perú, Publicación Especial 9: 4 p.

Romero, D.; Valencia K., Alarcón, P., Ramos, V.A. 2011. Geología de la costa pacífica del Perú central entre Chiclayo y Paracas (7°–14° Sur). 14 Congreso Latinoamericano de Geología, Memorias: 110–111. Medellín.

Romero, D.; Valencia K., Alarcón P., Peña D., Ramos, V.A. 2013. The offshore basement of Perú: Evidence for different igneous and metamorphic domains in the Forearc. Journal of South American Earth Sciences 42: 47–60. https://doi.org/10.1016/j.jsames.2012.11.003

Rossello, E.A.; Cossey, S., Fernandez, G. 2022. The hydrocarbon potential of the offshore Talara Basin, Peru. Andean Geology 49 (1): 1-17. http://dx.doi.org/10.5027/andgeoV49n1-3383

Rouillard, P.; Collot J., Sutherland R., Bache F., Patriat M., Etienne S., Maurizot P. 2015. Seismic stratigraphy and paleogeographic evolution of Fairway Basin, Northern Zealandia, Southwest Pacific: from Cretaceous Gondwana breakup to Cenozoic Tonga–Kermadec subduction. Basin Research: 1–24. https://doi.org/10.1111/bre.12144

Rutland R.W.R. 1971. Andean orogeny and ocean floor spreading. Nature 233: 252–255

Saller, A, H.; Noah J., Ruzuar A., Schneider R., 2004. Linked lowstand delta to basin-floor fan deposition, offshore Indonesia: Analog for deep-water reservoir systems, American Association of Petroleum Geologists Bulletin 88(1): 21–46. https://doi.org/10.1306/09030303003

Saller, A.H.; Werner, K., Sugiaman F., Cebastiant A., May R., Glenn D., Barker, C. 2008. Characteristics of Pleistocene deep-water lobes and their application to an upper Miocene reservoir model, offshore East Kalimantan, Indonesia. American Association of Petroleum Geologists Bulletin 92: 919–949. https://doi.org/10.1306/03310807110

Sangree, J. B.; Widmier, J.M.1977. Seismic stratigraphy and global changes of sea level, Part 9: Seismic interpretation of clastic depositional facies. *In* Seismic Stratigraphy — Applications to Hydrocarbon Exploration (Payton, C.E.; editor). American Association of Petroleum Geologists Memoir 26: 165–184. https://doi.org/10.1306/M26490C11

SAVIA 2014. Bio-Chrono Regional Stratigraphic Correlation – Sechura-Trujillo-Salaverry Basins, Internal report (Unpublished): 38 p.

Schell, W. 1978. Paleontology of Occidental wells, Peru: Occidental Petroleum Company Internal Report (Unpublished): 4 p.

Schrader, H.; Cruzado, J. 1990. The Ballena and Delfin wells off central Peru: Revised ages. *In* Proceedings of the ocean drilling program (Suess, E.; von Huene, E. R. et al.; editors), Scientific Results, 112: 209–215. DOI:10.2973/ODP.PROC.SR.112.187.1990

Seely, D.R. 1979. The evolution of structural highs bordering major forearc basins. *In* Geological and Geophysical Investigations of Continental Margins (Watkins, J.S.; Montadert, L.; Dickerson, P.W.; editors) Geological and Geophysical Investigations of Continental Margins. American Association of Petroleum Geologists Memoir 29: 245–260. https://doi.org/10.1306/M29405C17

Seely, D.R.; Vail, P.R., Walton, G.G. 1974. Trench slope model. *In* The Geology of Continental Margins (Burk, C.A.; Drake, C.L.; editors). Springer-Verlag: 249–260. New York. https://doi.org/10.1007/978-3-662-01141-6_18

Shew, R.D.; Rollins, D.R., Tiller, G.M., Hackbarth, C.J., White, C.D. 1993 Characterization and modeling of thin-bedded turbidite deposits from the Gulf of Mexico using detailed subsurface and analog data. *In* Submarine fans and turbidite systems - sequence stratigraphy, reservoir architecture, and production characteristics Gulf of Mexico and International (Weimer, P., Bouma, A.H., Perkins, B.E.; editors) SEPM Gulf Coast Section Publications 15: 327-334. https://doi.org/10.5724/gcs.94.15.0349

Snedden, J.W.; Kreisa, R.D., Tillman, R.W., Culver, S.J. and Schweller, W.J. 1999. An expanded model for modern shelf sand ridge genesis and evolution on the New Jersey Atlantic shelf. *In* Isolated Shallow Marine Sand Bodies: Sequence Stratigraphic Analysis and Sedimentologic Interpretation (Bergman, K.M.; Snedden, J.D.; editors). SEPM Society for Sedimentary Geology Special Publication 64:147–163. https://doi.org/10.2110/pec.99.64.0147

Steel, R. J. 1993. Triassic–Jurassic megasequence stratigraphy in the Northern North Sea: rift to post-rift evolution. Geological Society, London, Petroleum Geology Conference Series 4: 299 – 315. https://doi.org/10.1144/0040299

Sternbach, L.R. ; Bang, S., Bianchi, C., Cespedes, J., Han, Y., Choi, D.S., 2010. Offshore Peru, Trujillo Basin, Block Z-46: 2D PSTM Seismic Processing Reveals Deep Basins, Normal and Transtensional Faulting and Thick Eocene/Oligocene Stratigraphic Complex Submarine Fans Linked to Evidence of Hydrocarbons/DHI's. American Association of Petroleum Geologists Search and Discovery. Article #10263, 11 p.

Stewart, I. J. 2020. Tectonostratigraphic Megasequences and Chronostratigraphy. *In* Regional Geology and Tectonics, Volume 1: Principles of Geologic Analysis. Second Edition, Elsevier: 113-117. Amsterdam. https://doi.org/10.1016/B978-0-444-64134-2.00011-0

Suess, E. et al. 1988. Shipboard Scientific Party, 1988 Site 684. *In* Proceedings of Ocean Drilling Program, Leg 112 Initial Reports, Part A. Ocean Drilling Program:. 525–595. College Station. doi:10.2973/odp.proc.ir.112.1988

Suter, J.R. 2006. Facies models revisited: Clastic shelves. *In*: Facies Models Revisited (H.W. Posamentier H.W.; R.G. Walker, R.G.; editors) SEPM Society for Sedimentary Geology Special Publication 84: 339–397. https://doi.org/10.2110/pec.06.84.0339

Swift, D.J.P.; Field, M.E.,1981. Evolution of a classic sand ridge field: Maryland sector, North American inner shelf. Sedimentology 28: 461-482. https://doi.org/10.1111/j.1365-3091.1981.tb01695.x

Takano, O. 2017. Intermittent Formation, Sedimentation and Deformation History of Cenozoic Forearc Basins Along the Northwestern Pacific Margins as an Indicator of Tectonic Scenarios. *In* Dynamics of Arc Migration and Amalgamation–Architectural Examples From the NW Pacific Margin (Ito, Y; Takano, O.: Takashima, R.; editors). InTech, pp. 1–24. doi: 10.5772/intechopen.68290

Takano, O.; Itoh, Y., Kusumoto, S., 2013. Variation in Forearc Basin Configuration and Basin-filling Depositional Systems as a Function of Trench Slope Break Development and Strike-Slip Movement: Examples from the Cenozoic Ishikari–Sanriku-Oki and Tokai-Oki–Kumano-Nada Forearc Basins, Japan. *In* Mechanism of Sedimentary Basin Formation - Multidisciplinary Approach on Active Plate Margins (Itoh Y.; editor) InTech, chapter 1: 1-24. http://dx.doi.org/10.5772/56751

Takano, O.; Tsuji, T., Yamada, Y., Ijiri, A., Ishikawa, T., Murayama, M., Kondo, Y., Inagaki, F. 2025. Depositional Ages, Sequence Stratigraphy and Transition Process of Forearc Setting From Paleogene Restricted Bay/ Estuarine to Neogene Open- Marine Deltaic/Slope Systems in the Sanriku- Oki Forearc Basin, Northeast Japan. Basin Research 37, no. 4: e70042. https://doi.org/10.1111/bre.70042

Thornburg, T.M. 1985. Seismic stratigraphy of Peru forearc basins. *In* D.M. Hussong et al. (Eds.), Atlas of the Ocean Margin Drilling Program, Peru Continental Margin, Region VI (Hussong, D.M.et al.; editors). Marine Science International: 8 p. Woods Hole

Thornburg, T.; Kulm, L. D. 1981. Sedimentary basins of the Peru continental margin: Structure, stratigraphy, and Cenozoic tectonics from 6ºS to 16º latitude. *In* Nazca Plate: Crustal Formation and Andean Convergence (Kulm, L. D.; Dymond, J.; Dash, E. J.; Hussong, D. M.; editors). Geological Society of America Memoir 154: 393-422. https://doi.org/10.1130/MEM154-p393

Timoteo, D. 2013. Potencial Generador de Hidrocarburos y Distribución de las Secuencias Cretácicas costa afuera (offshore) del Perú centro–norte (Lima-Chiclayo). Tesis Título

Profesional de Ingeniero Geólogo (Unpublished). Universidad Nacional de Ingeniería, 226 p. Lima.

Timoteo, D. 2015. Sismo estratigrafia dos Depósitos Cenozóicos da Bacia Salaverry, porção offshore do Peru: Novas interpretações do sistema petrolífero. Dissertação de Mestrado N 356 (Unpublished), Instituto de Geociências, Programa de pós-graduação em Geologia, Universidade de Brasília:: 109 p.

Timoteo, D.; Valencia, K. 2014. Caracterização Geológica Geoquímica das rochas geradoras Cretácicas potenciais da Bacia Salaverry, Peru. 47 Congresso Brasileiro de Geologia, (Salvador), Anais: 1485.

Timoteo, D.; Chemale Junior, F., Borda, E. 2018. Seismic stratigraphy of Cenozoic deposits in the Salaverry forearc Basin, Peru: New insights in assessing potential reservoirs and plays. *In* Petroleum basins and hydrocarbon potential of the Andes of Peru and Bolivia (Zamora, G.; McClay, K. R.; Ramos, V.A. (eds.). American Association of Petroleum Geologists Memoir 117: 339–376. https://doi.org/10.1306/13622127M1173773

Vail, P. R.; Mitchum, R.M., Thompson, S. 1977. Seismic stratigraphy and global changes of sea level, Part 3: Relative changes of sea level from coastal onlap. *In* Seismic Stratigraphy — Applications to Hydrocarbon Exploration (Payton, C.E.; editor). American Association of Petroleum Geologists Bulletin Memoir 26: 83–98. https://doi.org/10.1306/M26490C5

Valdespino, T.; Seminario, F. 1976. Informe Micropaleontológico del pozo Ballena 8X–1: Petroperu, Reporte interno (Unpublished): 3 p.

Valdespino, T.; Seminario, F. 1976b. Informe Micropaleontológico del pozo Delfin 20X–1X: Petroperu, Reporte interno (Unpublished): 4 p.

Valencia, K.; Romero, D. 2011. Evolución Tectono-sedimentaria de la Cuenca Salaverry y su Implicancia en la Generación de Hidrocarburos. VII Seminario Internacional de Exploración y Producción de Petróleo y Gas – INGEPET:18. Lima.

Valencia, K.; Romero, D., Alarcón, P., Llerena, Borda, C.E., Rojas, J. 2013. Structural evolution of convergent margin of Central Peru and its relationship with petroleum systems of the forearc Salaverry Basin. American Association of Petroleum Geologists Search and Discovery Article #90166.

Van der Werfff, W. 1996 Variation in forearc basin development along the Sunda Arc, Indonesia, Journal of Southeast Asian Earth Sciences14(5): 331-349. https://doi.org/10.1016/S0743-9547(96)00068-2

von Huene, R.; Kulm, L., Miller, J., and Hussong, D., 1986. *In* Seismic Images of Modern Convergent Margin Tectonic Structure (von Huene, R., editor). American Association of Petroleum Geologists Studies in Geology 26: 37-42. https://doi.org/10.1306/St26461C8

Weimer, P.; 1991. Chapter 18. Seismic Facies, Characteristics, and Variations in Channel Evolution, Mississippi Fan (Plio-Pleistocene), Gulf of Mexico. In: Seismic Facies and Sedimentary Processes of Submarine Fans and Turbidite Systems (Weimer.; M. H. Link, M.H.; editors) Springer-Verlag: 323-347. New York. https://doi.org/10.1007/978-1-4684-8276-8_18

Williams, G.D. 1983.Tectonics and seismic sequence stratigraphy: an introduction. *In* Tectonics and Seismic Sequence Stratigraphy (Williams, G. D.; A. Dobb, A., editors). Geological Society London Special Publication 71: 1-13. https://doi.org/10.1144/GSL.SP.1993.071.01.01

Wine, G.; Arcuri, J., Martínez, Monges, E.C., Calderón, Y., Galdos, C., 2001. Hydrocarbon potential of the Salaverry offshore Basin Peru: PeruPetro Internal Report (Unpublished): 67p.

Witt, C.; Alarcón, P., Valencia, K., Lajo, A., Fuentes, J., Romero, D. 2011. Segmentación tectono-estratigráfica y superposición de cuencas de antearco cenozóicas en la margen andina entre 6°S y 2°S (Norte Perú e Sur Ecuador). 14 Congreso Latinoamericano de Geología, Memorias: 248–249. Medellín.

Witt, C.; Bourgois, J. 2009. Forearc basin formation in the tectonic wake of a collision-driven, coastwise migrating crustal block: The example of the North Andean block and the extensional Gulf of Guayaquil-Tumbes Basin (Ecuador-Peru border area). Geological Society of America Bulletin, 122(1-2): 89–108. https://doi.org/10.1130/B26386.1

Wynn, R. B.; Cronin, B. T., Peakall, J., 2007. Sinuous deep-water channels: Genesis, geometry and architecture. Marine and Petroleum Geology 24(6-9): 341–387. https://doi.org/10.1016/j.marpetgeo.2007.06.001

Zulkifli, Z.; Clare, M.A., Heijnen M., Lintern G., Stacey C., Talling P.J., Cartigny M.J.B., Minshull T.A., Marin Moreno H., Peakall J., Darby, S. 2024. A threshold in submarine channel curvature explains erosion rate and type, Earth and Planetary Science Letters 646: 118953. https://doi.org/10.1016/j.epsl.2024.118953

Zuñiga-Rivero, F.; Keeling, J., Hay-Roe, H. 1998. Peru onshore-deepwater basins should have large potential. Oil Gas Journal, 96 (42).